# Дифракция нейтронов и синхротронного излучения: применение для исследования упругой анизотропии горных пород

Роман Васин

Лаборатория нейтронной физики им. И.М. Франка

Объединённый институт ядерных исследований

Г. Дубна, Россия

Seismic waves and bulk elastic properties of rocks

Study of elastic waves propagating through the Earth is necessary to derive models of Earth's internal structure; models/prognosis of earthquakes; geophysical prospecting (e.g., oil and gas deposits).

Exploring the Earth using Seismology

	(Lat, Long, dt2)
	(12.5° N, 40.0° E, 1.3)
	(10.0° N, 41.0° E, 1.1)
	(9.5° N, 70.0° W, −0.2)
	(12.8° N, 86.5° W, −1.6)
	(11.0° N, 85.0° W, 0.0)

PKIKP^2(I2)   PKIIKP^2(II2)

Travel time (s)

http://www.iris.edu/hq/
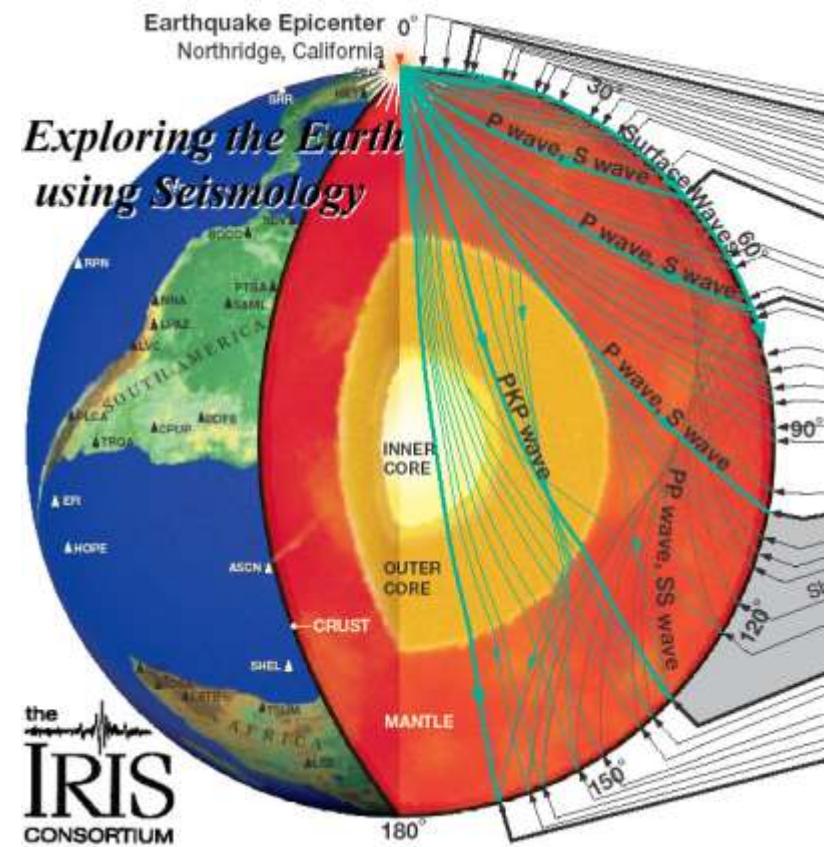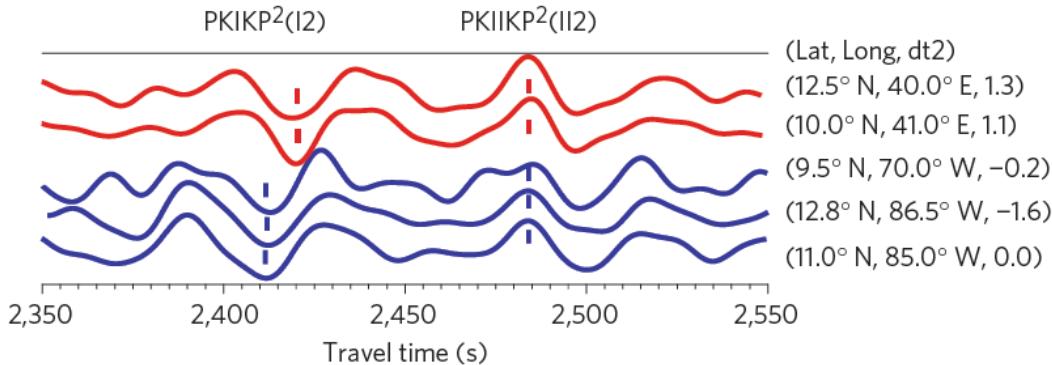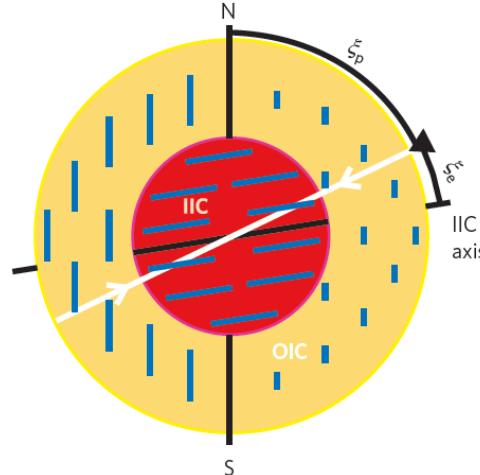
The Earth's inner core is solid and exhibits strong elastic anisotropy due to the preferred orientation of iron crystallites. Recently, observations of seismic waves resulted in a two-component inner core model with different anisotropy types of both components.

Seismic waves and bulk elastic properties of rocks

Study of elastic waves propagating through the Earth is necessary to derive models of Earth's internal structure; models/prognosis of earthquakes; geophysical prospecting (e.g., oil and gas deposits).
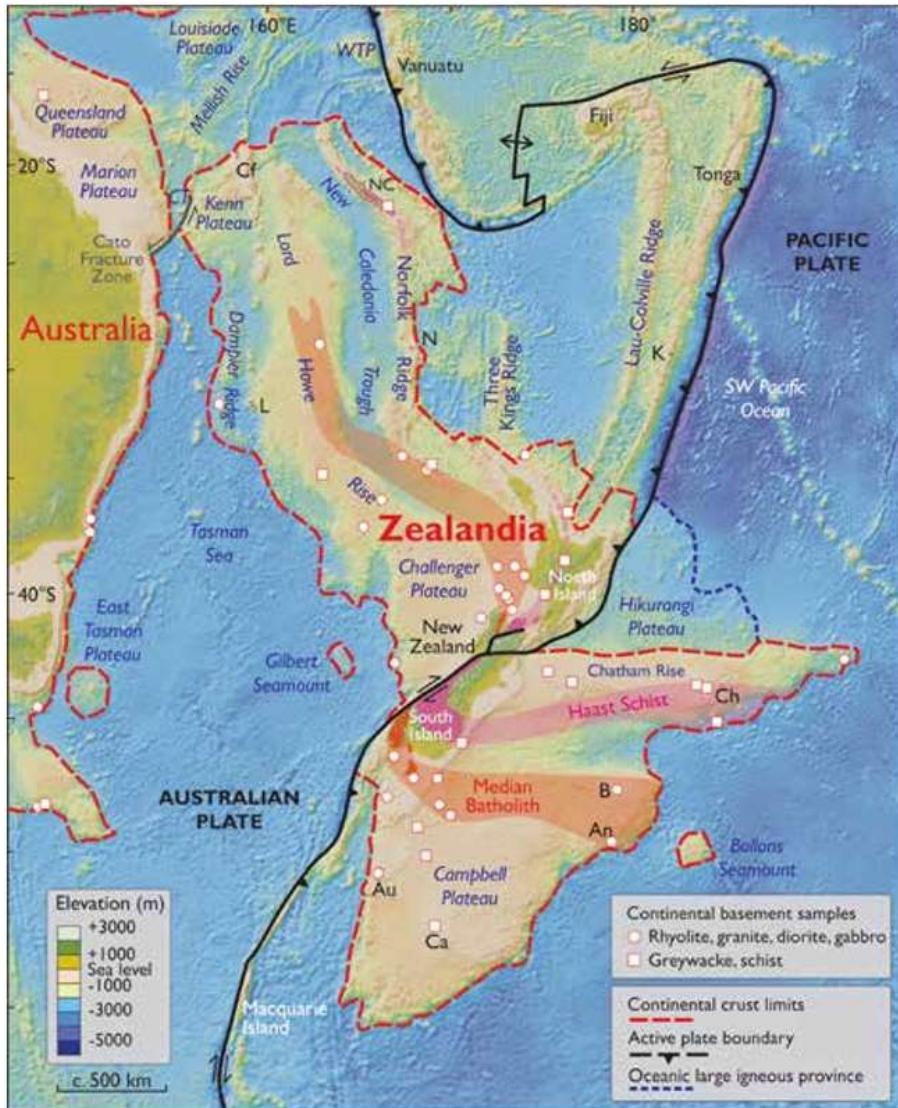

Figure 2. Spatial limits of Zealandia. Base map from Stagpoole (2002) based on data from Smith and Sandwell (1997). Continental basement samples from Suggate et al. (1978), Beggs et al. (1990), Tulloch et al. (1991, 2009), Gamble et al. (1993), McDougall et al. (1994), and Mortimer et al. (1997, 1998, 2006, 2008a, 2008b, 2015). NC—New Caledonia; WTP—West Torres Plateau; CT—Cato Trough; Cf—Chesterfield Islands; L—Lord Howe Island; N—Norfolk Island; K—Kermadec Islands; Ch—Chatham Islands; B—Bounty Islands; An—Antipodes Islands; Au—Auckland Islands; Ca—Campbell Island. Mercator projection.

N. Mortimer et al. (2017). GSA Today, DOI: 10.1130/GSATG321A.1

"A 4.9 Mkm^2 region of the southwest Pacific Ocean is made up of continental crust. The region has elevated bathymetry relative to surrounding oceanic crust, diverse and silica-rich rocks, and relatively thick and low-velocity crustal structure…
The identification of Zealandia as a geological continent, rather than a collection of continental islands, fragments, and slices, more correctly represents the geology of this part of Earth…"

Crystallographic texture

Many materials (metals, ceramics, rocks,…) are polycrystals; they consist of grains (crystallites) of different shape, size and orientation.

Crystallographic texture is the lattice (or crystallographic) preferred orientation of crystallites of some phase (e.g., one or other mineral in case of the multimineral rock) in the chosen (macroscopic) coordinate system.

Common abbreviation: LPO (or CPO).
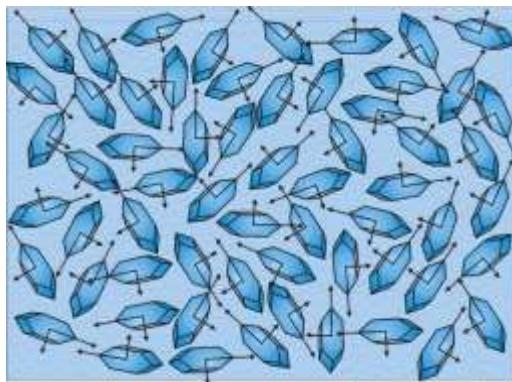
Random/chaotic orientation:
NO crystallographic texture
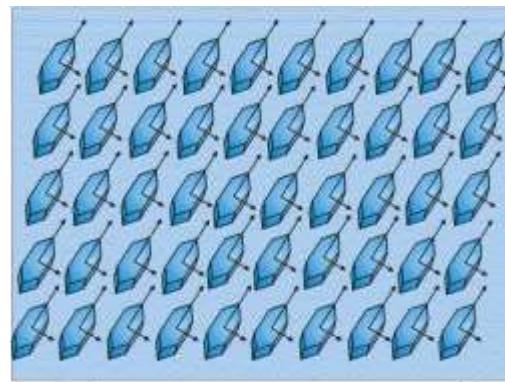
Aligned grains:
One-component
crystallographic texture
(≈ single crystal)
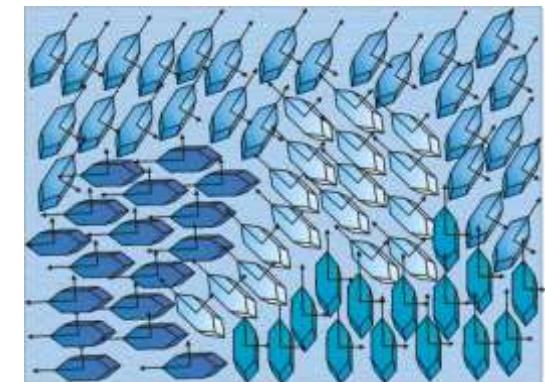
Multi-component
crystallographic texture
(different colors =
different orientations, not
different phases!)

Crystallographic texture is:

• a factor of «genetic memory» about the deformation and metamorphic processes (crystallization, recrystallization, plastic deformation, sedimentation, …);
→ Its possible to deduce what processes formed a certain rock!

• one of the factors controlling physical properties of polycrystalline materials and their anisotropy.
→ Its possible to calculate elastic, plastic, thermal, magnetic, … properties of the polycrystal!

Peculiarities of the texture formation and texture types are influenced by:

• *type of the stress tensor* (confining pressure, uniaxial compression, three-axial compression, simple shear, flat stress state, etc.).

• *temperature conditions* (temperature, rate of temperature change, temperature gradient, etc.).

• *polymorphism* (structural phase transitions, transformation superplasticity, twinning, etc.).

• …

A possibility to study the 'history' of rock-forming processes

Stolpen, Germany. Columnar basalt.

Ingeborgfjellet, Norway. Massively folded strata.
Photo: Ólafur Ingólfsson 2004.
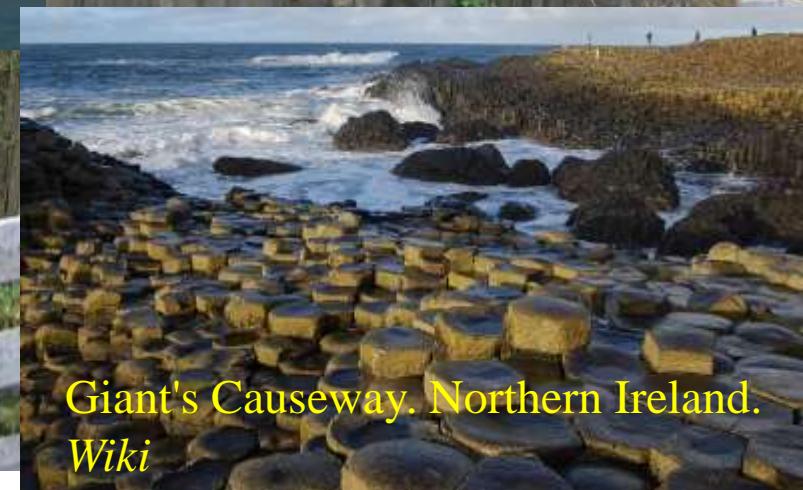
Giant's Causeway. Northern Ireland.
Wiki

Crystallographic texture as a way to deduce the deformation history

Measured LPO

Initial state (≈ random texture)

Uniaxial compression ($\varepsilon_{33} = -1.53$, $\sigma \approx 400$ MPa)
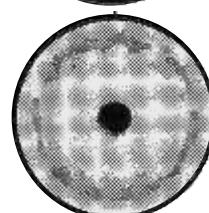
Uniaxial tension ($\varepsilon_{33} = 0.37$, $\sigma \approx 300$ MPa)
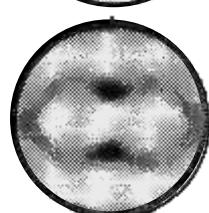
Flat compression ($\varepsilon_{11} = 0$, $\varepsilon_{33} = -1.54$, $\sigma \approx 350$ MPa)
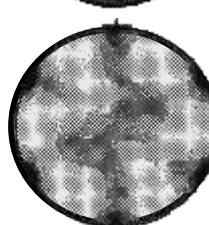
Simple shear ($\gamma_{12} = -1.40$, $\sigma \approx 150$ MPa)

Experimental pole figures (111) of the copper sample, T = 25ºC, strain rate = 0.001 s^{-1}.

*C.A. Bronkhorst et al. (1991) Textures and microstructures 14-18,1031-1036.*
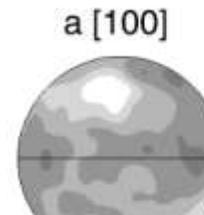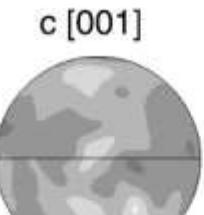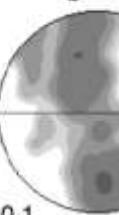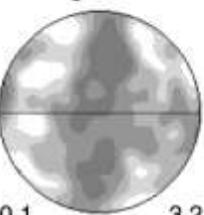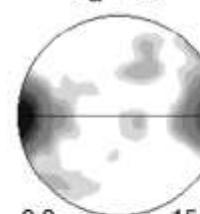
Experimental pole figures of olivine, deformed in dextral shear; different shear strain.

*M. Bystricky et al. (2000). Science 290, 1564-1567.*

Bulk physical properties of polycrystals

Crystallographic texture is one of the factors controlling physical properties of polycrystalline materials and their anisotropy. Elastic properties of the single crystal + measured Orientation Distribution Function could be combined to estimate elastic properties of polycrystal.
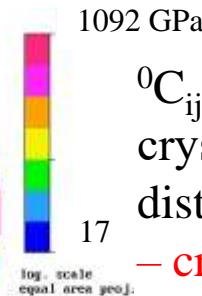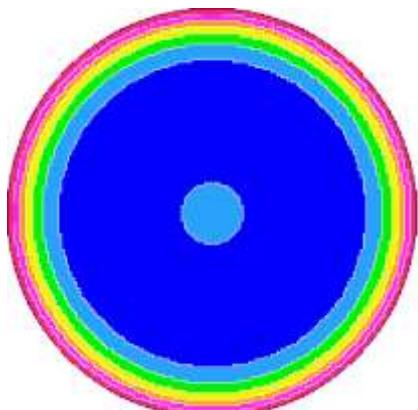
$^0C_{ijkl}$ of graphite single-crystal (Young's modulus distribution is plotted in K_B – crystal coordinate system)

Knowledge of single crystal properties is essential!!

Averaging procedures
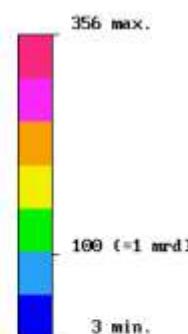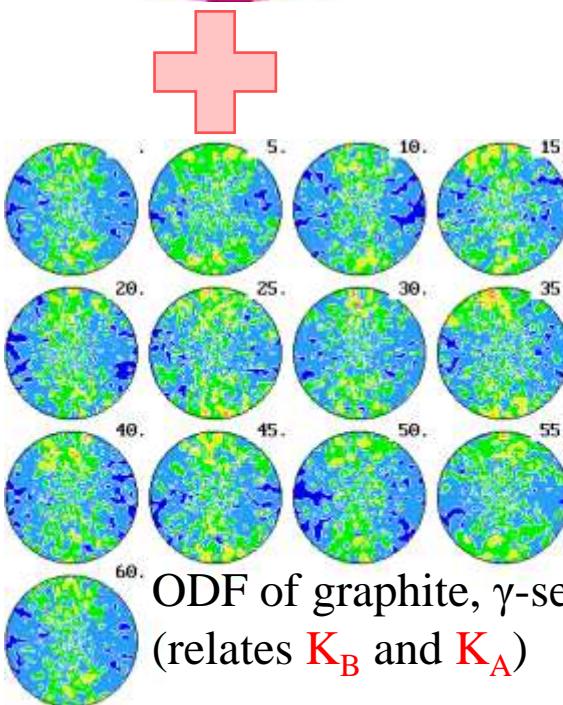
ODF of graphite, γ-sections (relates K_B and K_A)

T. Lokajicek et al. (2012). Carbon 49, 1374-1384.
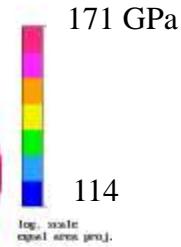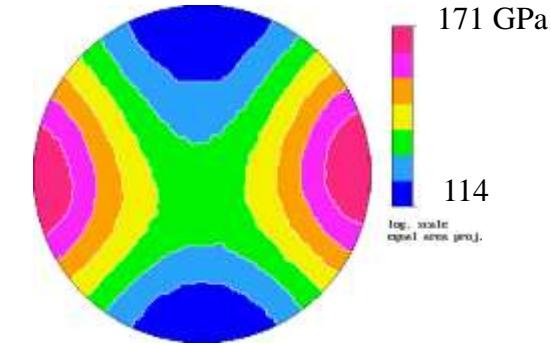
C_{ijkl} of graphite polycrystal with measured ODF, GEO average (Young's modulus distribution is plotted in K_A – sample coordinate system)

Bulk elastic properties of rocks and seismic waves

Study of elastic waves propagating through the Earth is necessary to derive models of Earth's internal structure; models/prognosis of earthquakes; geophysical prospecting (e.g., oil and gas deposits).


Post-perovskite pole figures along tracer #189, based on plasticity model assuming (001) slip
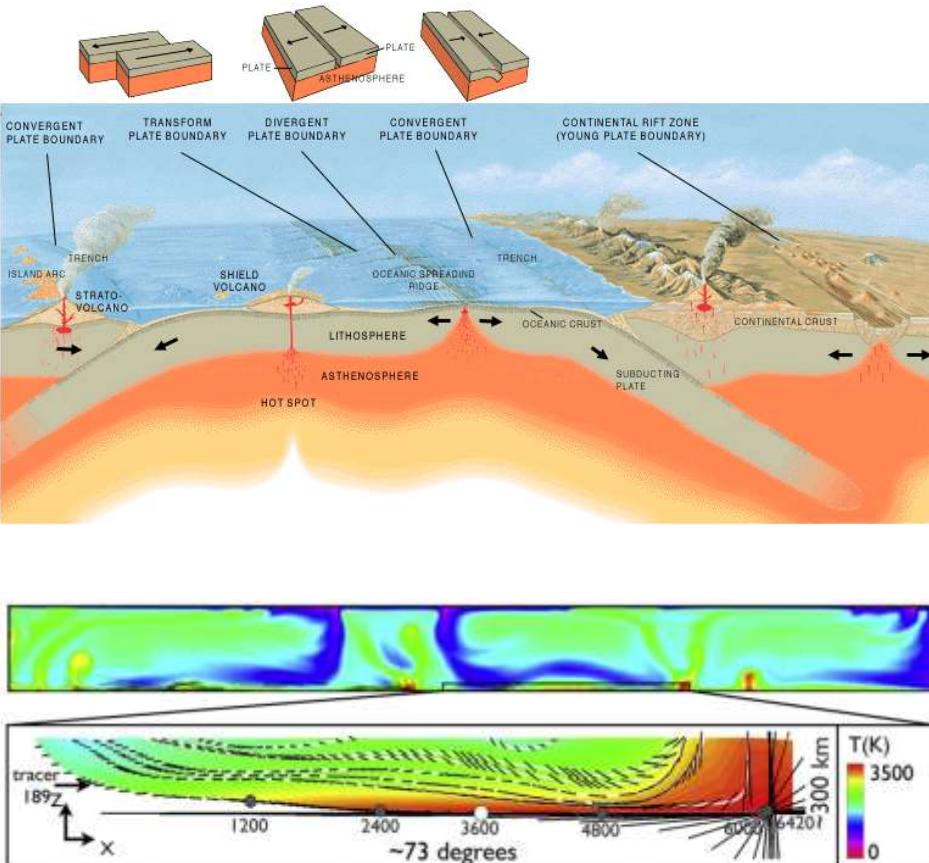
Geodynamic model – convection cell – in the lower mantle (D").

H.-R. Wenk et al. (2011). EPSL 306, 33-45.
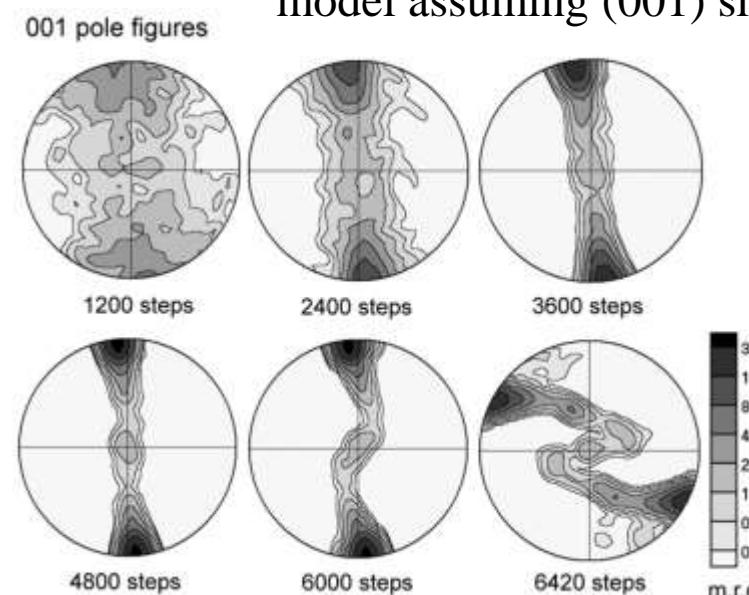
Dominant (001) slip in post-perovskite combined with {110} and {111} slip in magnesiowuestite best explains the seismic observations: high anisotropy and polarization of fast S-waves parallel to the CMB, as well as anti-correlation between P and S-wave anisotropies.

Orientation distribution function (ODF)

Each grain of the polycrystal possesses its own orientation g (defined, e.g., by 3 Euler angles).

Let dV be the total volume of grains of orientation g within dg interval, and let V be the total volume of the polycrystal (the same reasoning could be applied for the mass element – dm).

The 3D ODF $f(g)$ is defined as

$$\frac{dV}{V} = f(g)dg$$

It is normalized to unity:

$$\int_G f(g)\,dg = \frac{1}{8\pi^2} \int_0^{2\pi} d\alpha \int_0^{\pi} \sin\beta\,d\beta \int_0^{2\pi} f(\{\alpha,\beta,\gamma\})d\gamma = 1$$

ODF is the probability density to find the volume element of the sample with the orientation g within dg interval.
This infers that ODF is nonnegative!

Extreme cases:

random distribution $\qquad\qquad$ $f(g) = 1$

single-crystal $\qquad\qquad$ $f(g) = \delta\,(g_0)$

Pole figures

Pole figure (PF) is the angular distribution of some chosen crystallographic direction (e.g., normal to the {hkl} planes) in the sample coordinate system, mapped on the crystallographic (stereographic, equal area, …) projection.

Meaning in the texture analysis: the distribution of the probability density to find the volume element with {hkl} normal ‖ to different directions in the material (i.e., it is the ODF integrated over a certain path in the orientation space). Usually presented as contours of the "pole density" on the projection.

$\{hkl\}=\mathbf{h}$

001 **110**

Y_A

Z_A $\mathbf{y}$ X_A

0.12   4.95   0.26   2.04
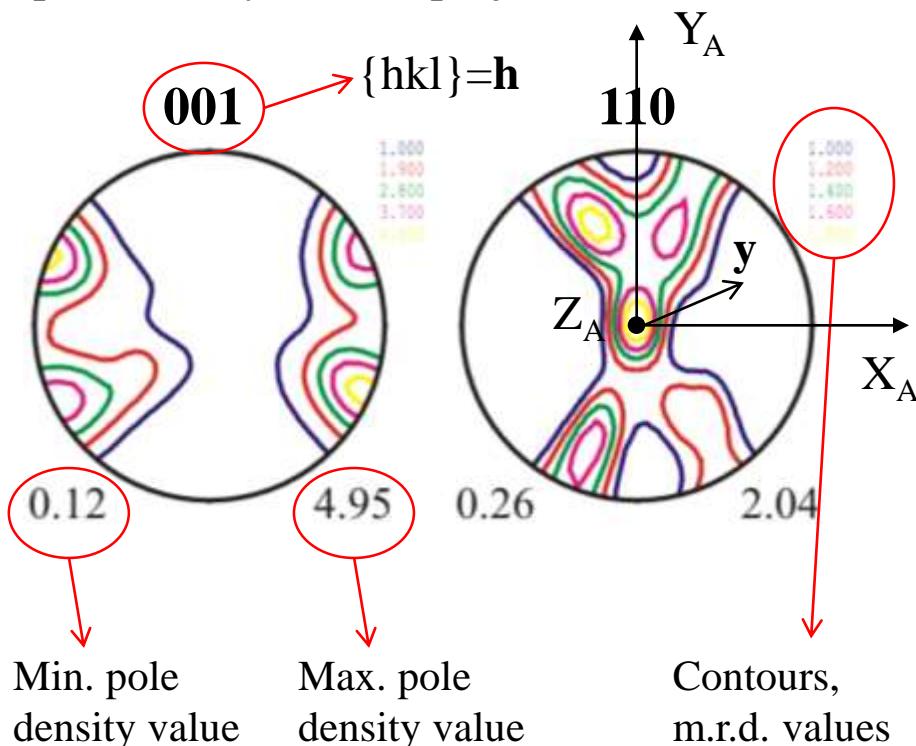
~ integral intensity of the diffraction peak

| Min. pole density value | Max. pole density value | Contours, m.r.d. values |

$$P_{\boldsymbol{h}}(\boldsymbol{y}) = \frac{1}{2\pi} \int_0^{2\pi} f(\{\boldsymbol{h}, \tilde{\varphi}\}^{-1}\{\boldsymbol{y}, 0\})\, d\,\tilde{\varphi}$$

+ Normalization!
(so absolute peak intensity is not important)
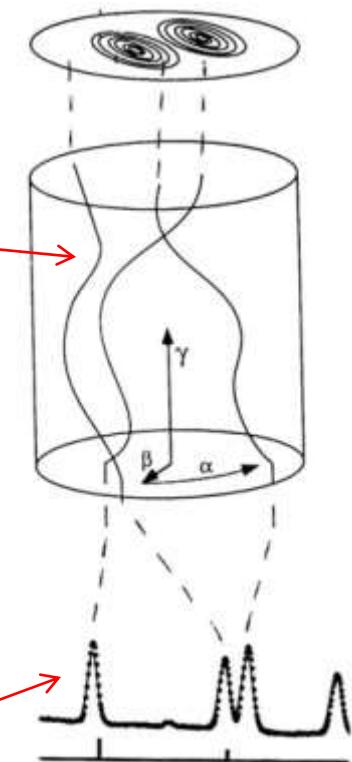
Pole figures
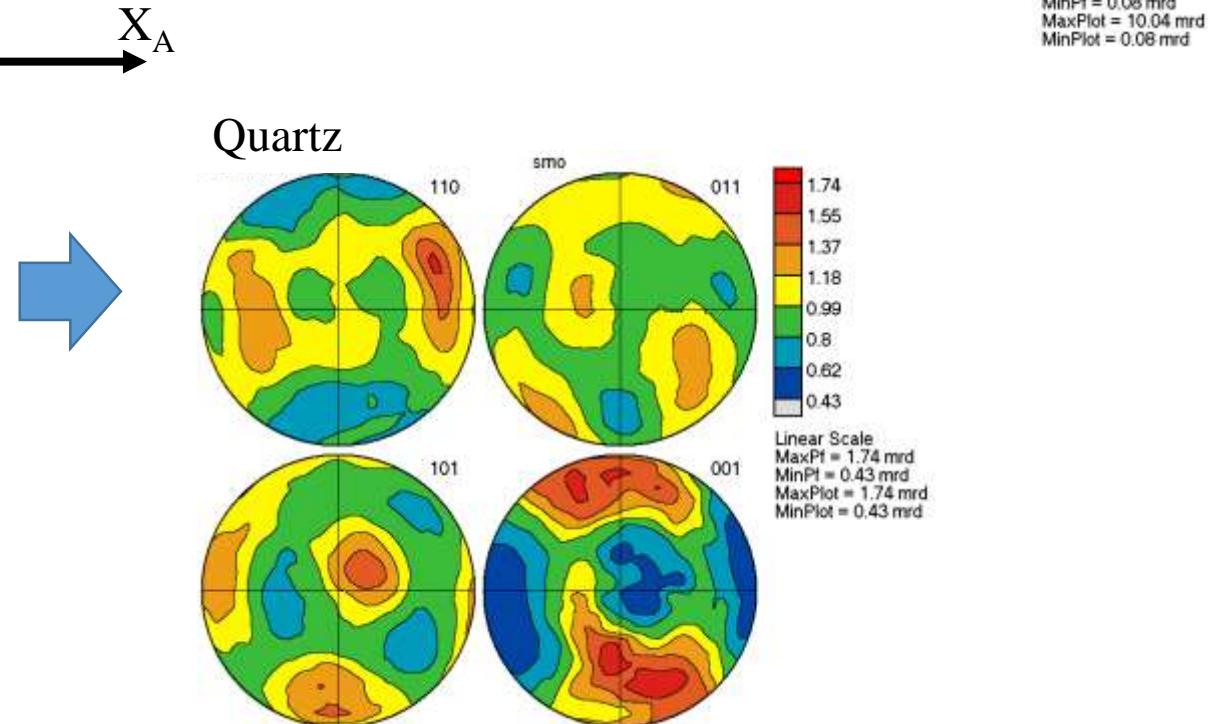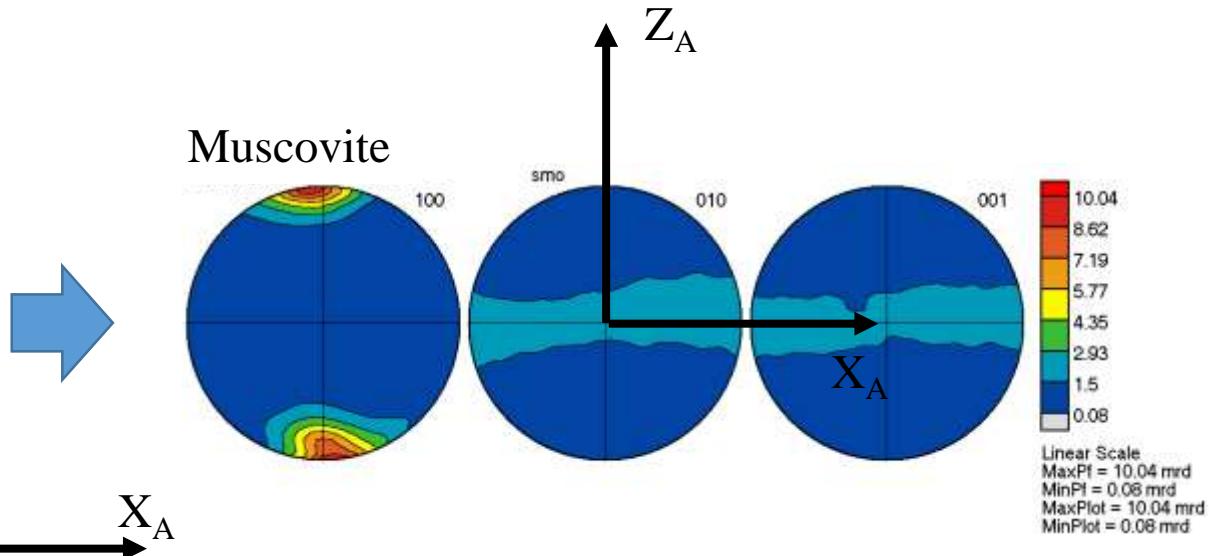
Inverse pole figures
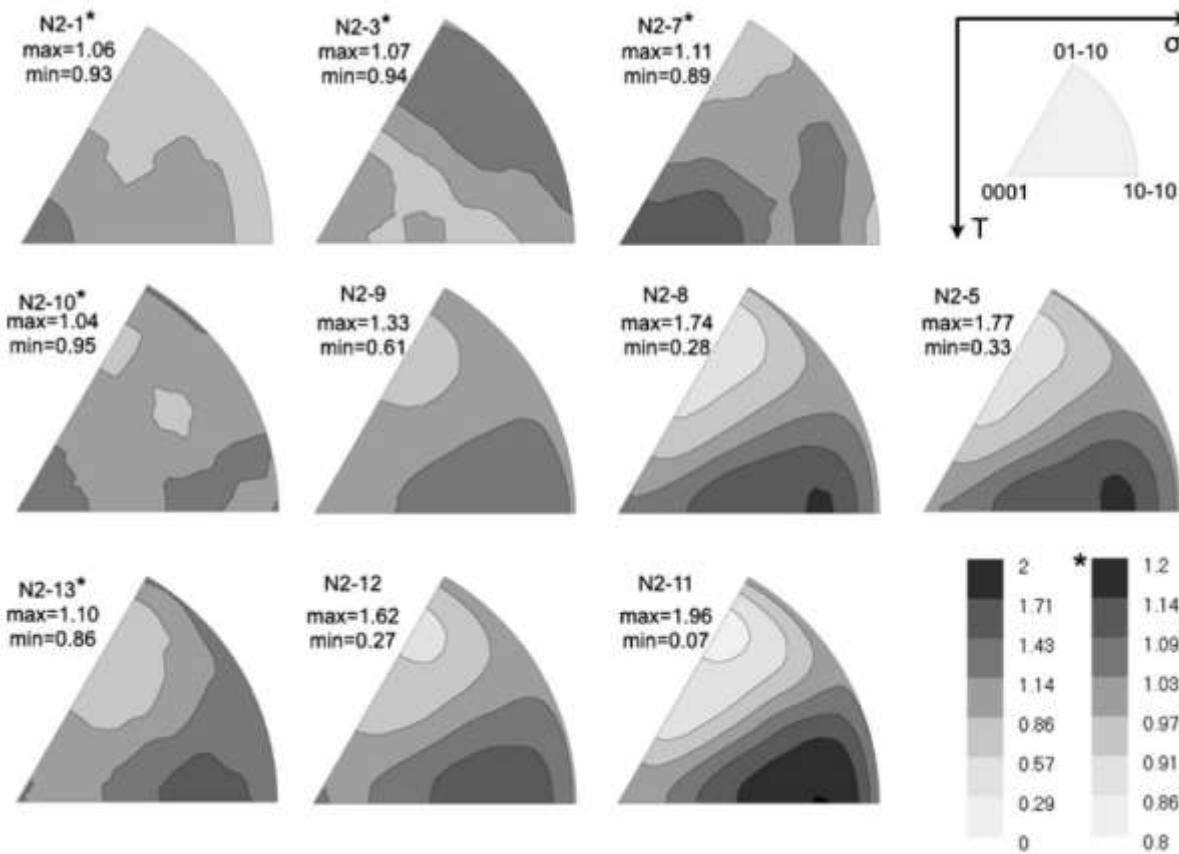
The distribution of the probability density to find the volume element, for which a chosen direction in the material || to different crystallographic directions. Usually presented as contours of the "pole density" on the projection.

Inverse pole figures of α-quartz (trigonal!) in uniaxially deformed (different p,T conditions) novaculite. Compression direction. Equal area projection.

Wenk H.-R., Rybacki E., Dresen G. et al. Dauphine twinning and texture memory in polycrystalline quartz. Part I: Experimental deformation of novaculite. // Phys. Chem. Minerals. 2006. V. 33. №10. P. 667-676.

Measuring the texture

1. Measure the orientation and the volume of each grain by optical or electron microscopy (only surface/or we need to destroy the sample…) → get the ODF as a set of Dirac delta functions with corresponding "weights".

2. Use diffraction to measure several pole figures → somehow derive 3D ODF out of finite number of its flat integral projections (PFs).

$$2d \cdot \sin \theta = n\lambda$$
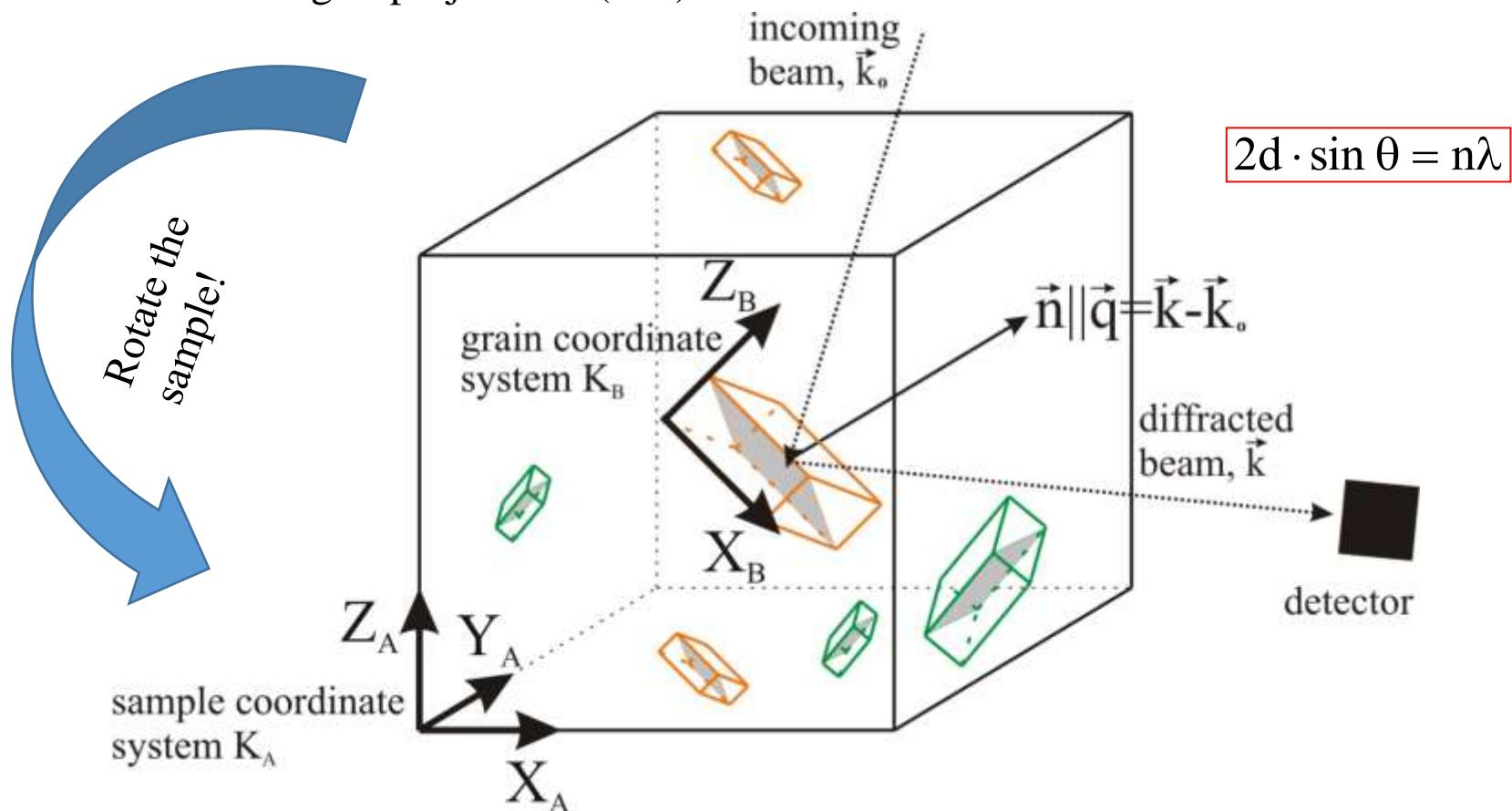
Why the diffraction (and specifically, neutron diffraction)?

- bulk texture investigation (linear dimensions of samples are ~ several cm);
- very high grain statistics: hundreds of thousands or millions of grains (necessary to get truly quantitative description of ODFs of all minerals composing the rock with 5°x5°x5° or better resolution);
- complex sample environments (low/high temperatures, high pressures, etc.);
- no special sample preparation;
- TOF (time-of-flight neutron diffraction on pulsed sources): each TOF spectrum contains information on one inverse pole figure. Using TOF it is possible to make a "bargain": measure more PF but with a lower angular resolution (less data on each PF → less sample rotations → less experimental time).
- neutron diffraction experiments started with minerals!

Table 1
Pole figure maxima and minima for antigorite in multiples of random distribution (m.r.d.).

	Antigorite (100)		Antigorite (010)		Antigorite (001)	
	Max.	Min.	Max.	Min.	Max.	Min.
Serpentinite A						
U-stage	22.8	0.0	35.5	0.0	31.6	0.0
EBSD	7.2	0.0	12.5	0.0	19.1	0.0
EBSD (manual)	13.1	0.0	26.3	0.0	12.3	0.0
Serpentinite B						
U-stage ~ 10^2	13.4	0.0	34.1	0.0	20.2	0.0
EBSD ~ 10^4	5.1	0.0	8.8	0.0	9.6	0.1
X-ray ~ 10^6	2.4	0.6	5.9	0.2	6.0	0.2
Serpentinite C						
X-ray	1.6	0.7	2.6	0.4	4.2	0.3

Grain size < 5μm

*Y. Soda, H.-R. Wenk (2014) Tectonophysics **615–616** 199–212.*

A bit of History

Ernest Omar Wollan

Clifford Glenwood Shull (The Nobel Prize in Physics 1994)

A double-crystal neutron spectrometer,
installed on the ORNL graphite reactor in 1949.

T.E. Mason et al. (2013). Acta Cryst. A69, 37-44

Lyle Benjamin
Borst,
first director of
ANL (Argonne)

*http://www.biography
ofpeople.com/borst-
lyle-benjamin-
biography*

A bit of History
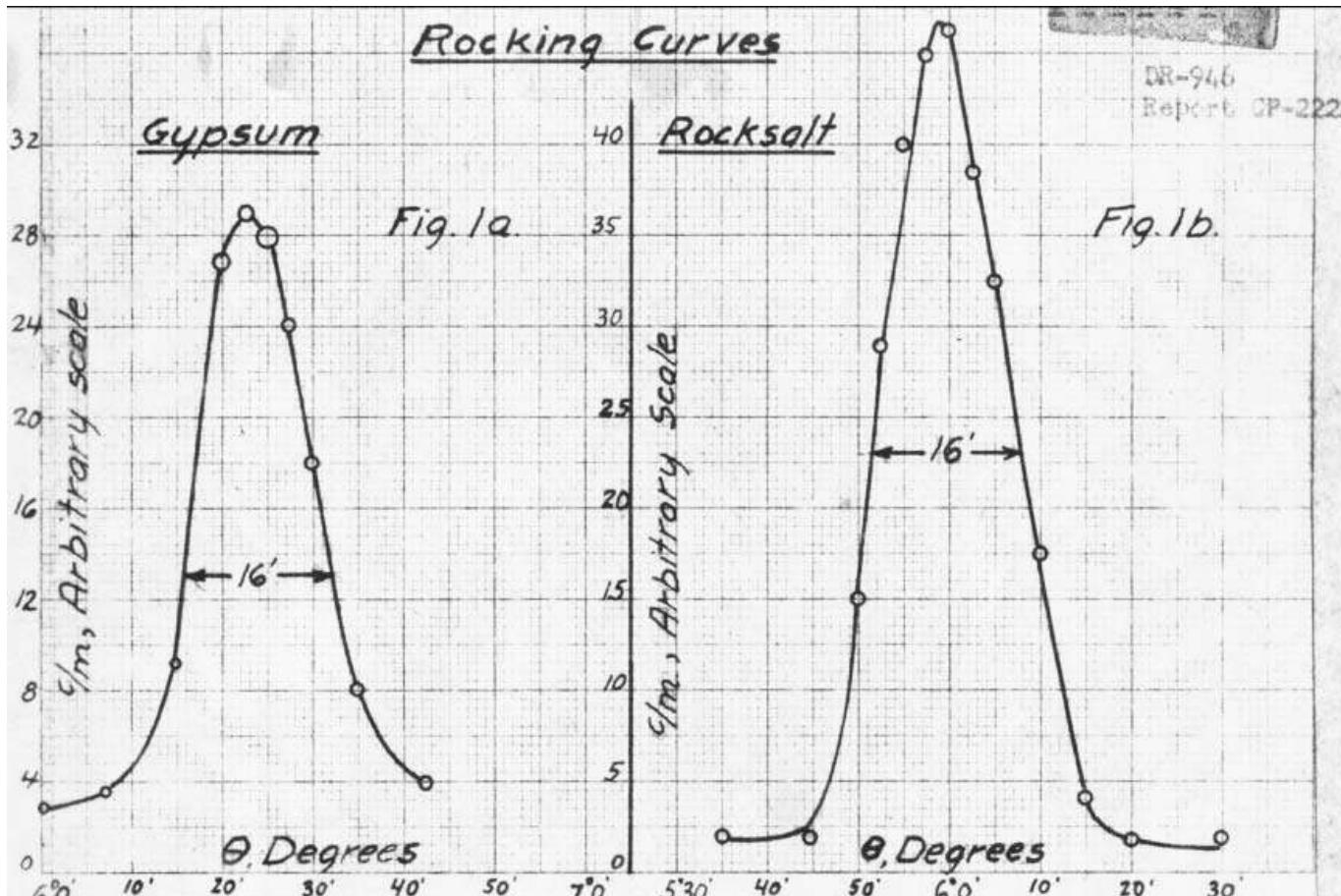
Gypsum
&
Halite (*Wiki*)
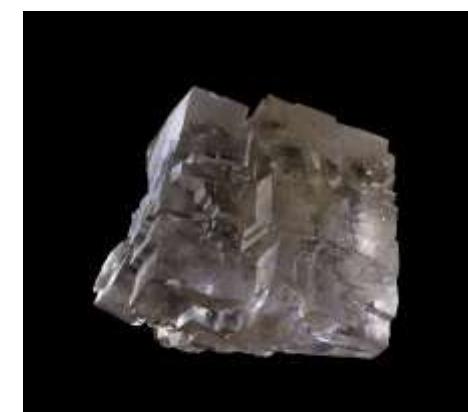
Wollan & Borst's first neutron diffraction results from December 1944; typical rocking curve experiments.

Diffraction patterns are fingerprints of crystal structures. The number of peaks and their positions tell about symmetry and size of the unit cell. Peak intensities depend on atom positions in the unit cell.

A bit of History

Zinn's first results from August 1944, CP-3 heavy water reactor, Argonne Lab.

Walter Henry Zinn, a photo back from 1946.

Don't you see something weird on the picture?

Why neutron scattering?

C.G. Shull and E.O. Wollan (1948). Science. 108, 69-75.

"The newly developing field of neutron diffraction would appear to have advantages over the older fields of X-ray and electron diffraction in some problems involved in the determination of crystal and molecular structures… It must be borne in mind, however, that really rapid progress along this line cannot be expected, …; also, the very limited facilities for work in this field which result from the requirement of a chain-reacting pile as a source will make progress less rapid than in the corresponding fields of X-ray and electron diffraction, for which adequate sources can be procured by any laboratory".

C.G. Shull et al. (1948). Phys. Rev. 73, 842-847.

"…crystallographic analysis of hydrogen atom positions should be readily possible."
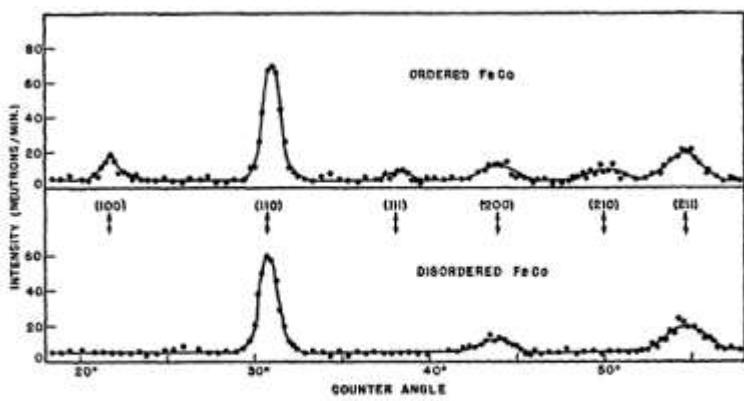

FIG. 8. Neutron powder diffraction patterns taken with samples of ordered and disordered preparations of Fe-Co alloys.
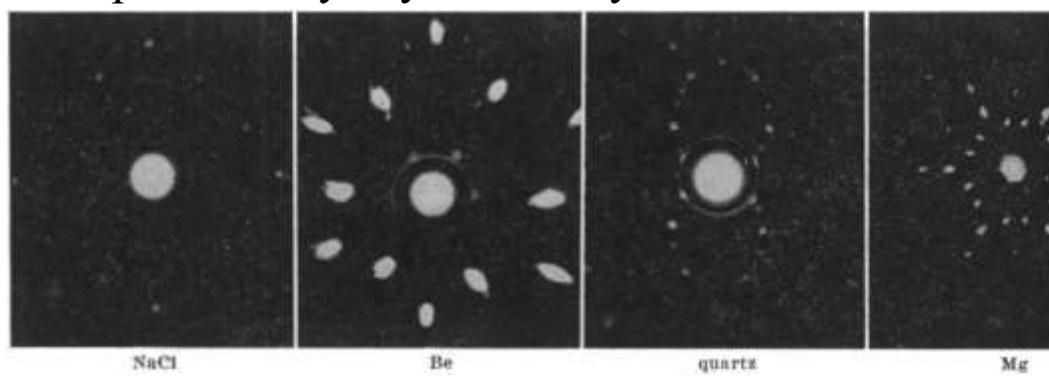
Laue photographs, first three (NaCl, Be, quartz) are made with neutrons, fourth is made with X-rays.

Neutron scattering in geography

Crystal Sound

Most of features named
after scientist who used
neutron diffraction to
study the structure of ice
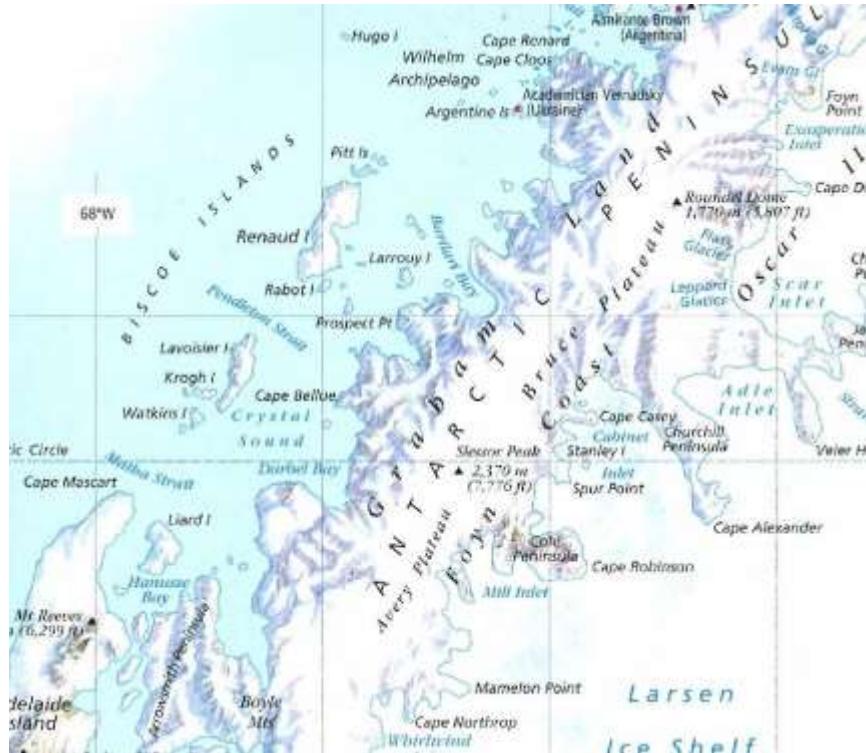
- Shull Rocks
- Pauling Islands
- Levy Island
- Wollan Island
- Davidson Island
- Matsuyama Rocks
- Fowler Islands
- …

SKAT texture diffractometer in FLNP JINR

Beamline 7a of IBR-2.

Main objectives: investigation of crystallographic textures of rocks (and engineering materials).
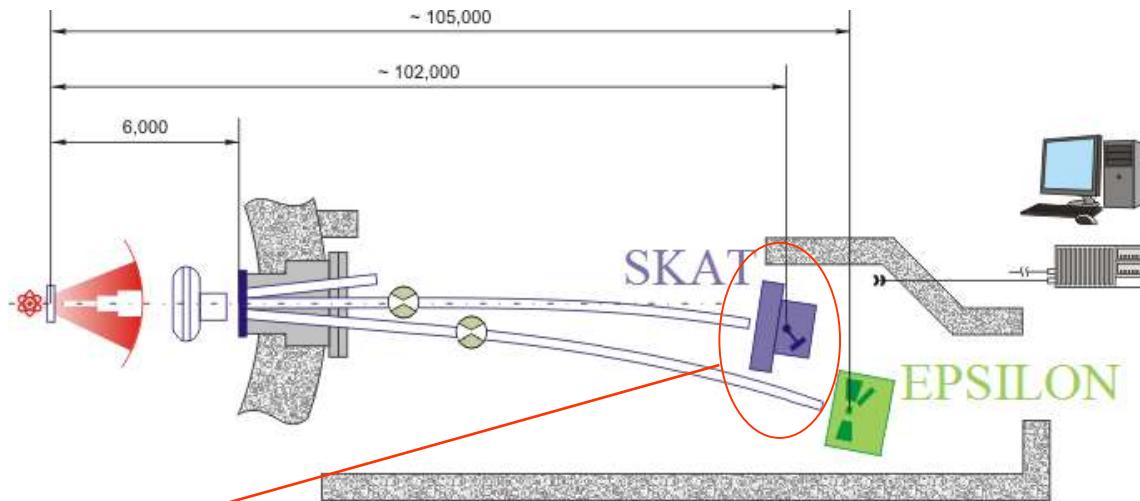
K. Ullemeyer et al. (1998). NuclearInst.Meth.A 412, 80-88.
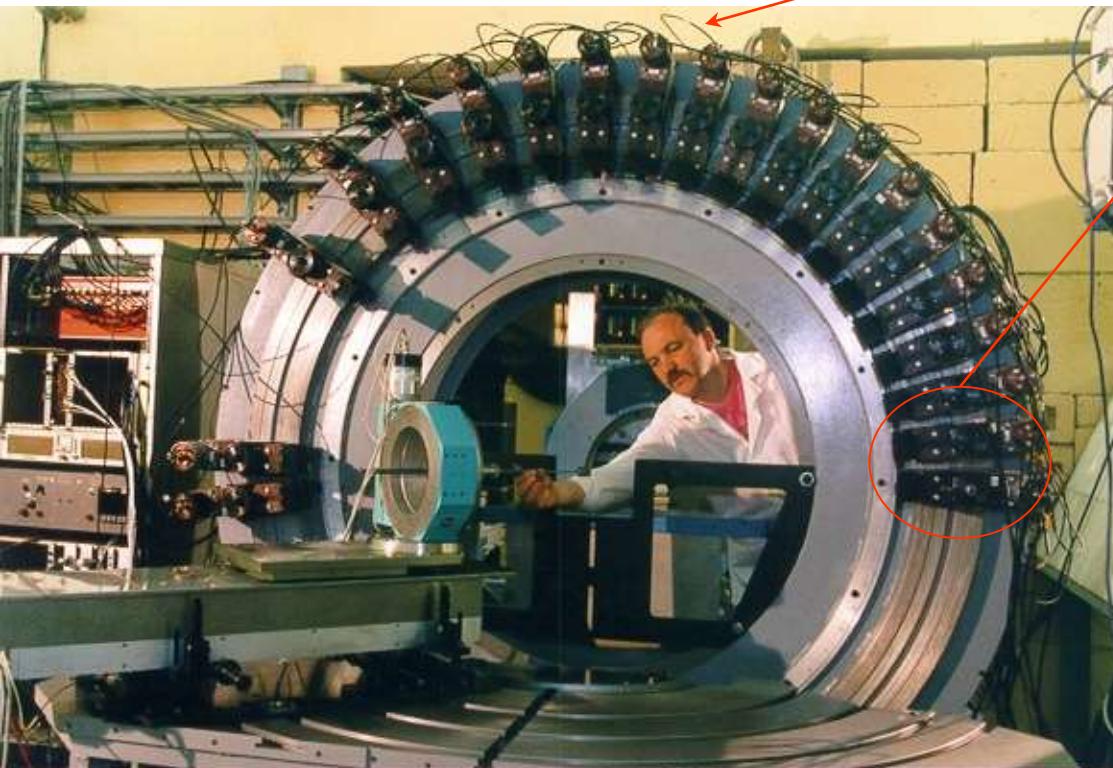
Total flight path: ≈ 104 m.

19 ^{3}He detectors on the mounting ring, unique scattering angle of $2\theta = 90°$.

Range of d-spacings: 0.5-5.4 Å (with 90° ring & w/o λ-chopper).

Resolution $\Delta d/d$ up to 0.55% ($d \approx$ 2.2 Å) with 18` collimators.

Sample size up to 5x5x5 cm^3.

(*Usually*) 1368 spectra from sample.

IBR-2 pulsed reactor at
Frank Laboratory of Neutron Physics of JINR

http://flnp.jinr.ru/

SKAT texture diffractometer: after the upgrade
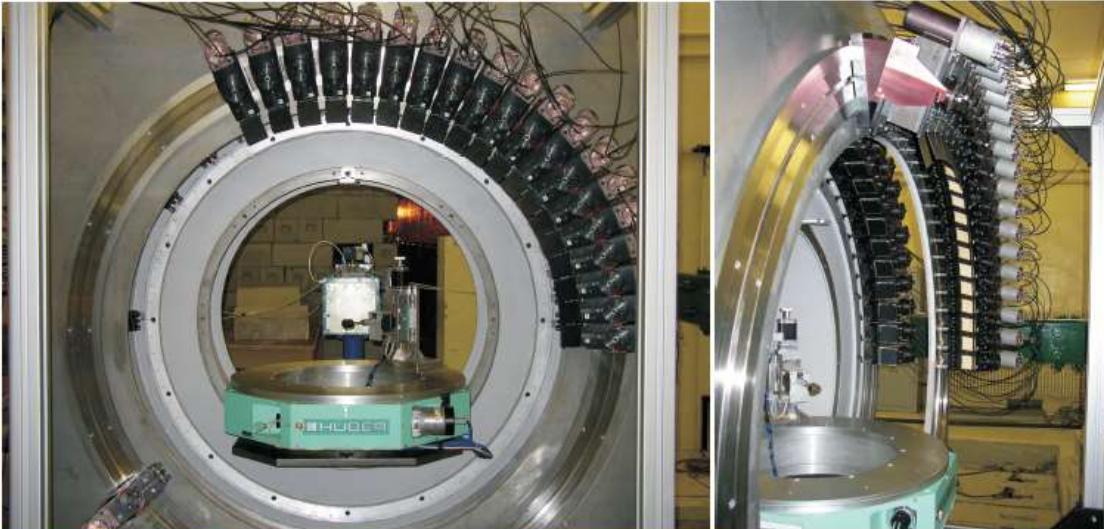
August 2012

Detector system
2Θ = 65°
(operational)

Detector system
2Θ = 135°
(detector holders

Legend:
- 2004 Sep., 18°
- 2013 Dec., 45°
- 2014 Jun., 45°
- 2004 Sep., 45°

Intensity (a.u.) vs TOF channel
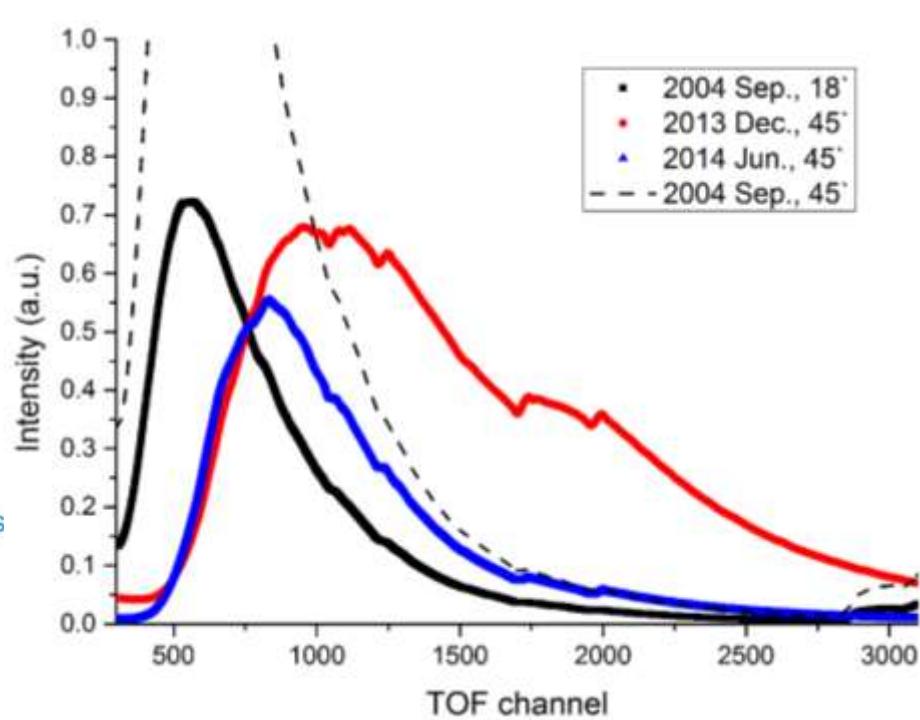
TOF texture diffractometers
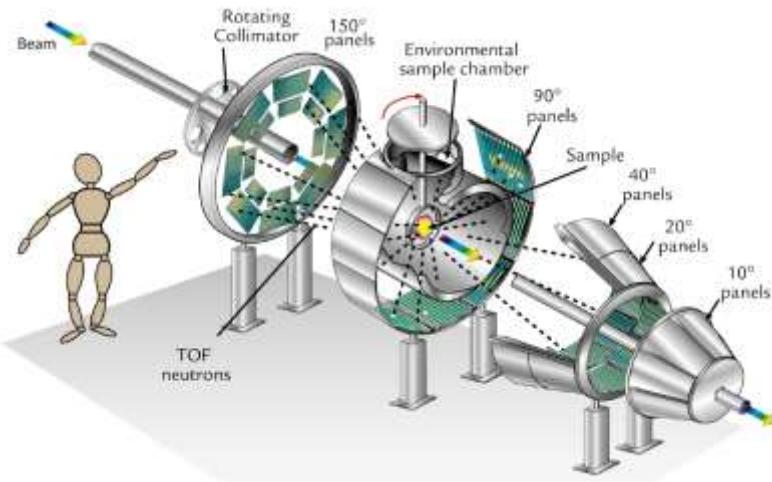
HIPPO diffractometer (LANSCE)

d-resolution: 0.4-9.2%
Flight path ~ 10 m
Sample dimensions ~ 2.5 cm
Range of *d*-spacings: 0.12-47.5 Å

*H.-R. Wenk et al. (2003) Nuclear Inst. Meth. A **515**, 575-588.*

iMATERIA (J-PARC)

d-resolution: 0.16-5.0%
Flight path ~ 30 m
Range of *d*-spacings: 0.09-800 Å

*T. Ishigaki et al. (2009) Nuclear Inst. Meth. A **600**, 189-191.*
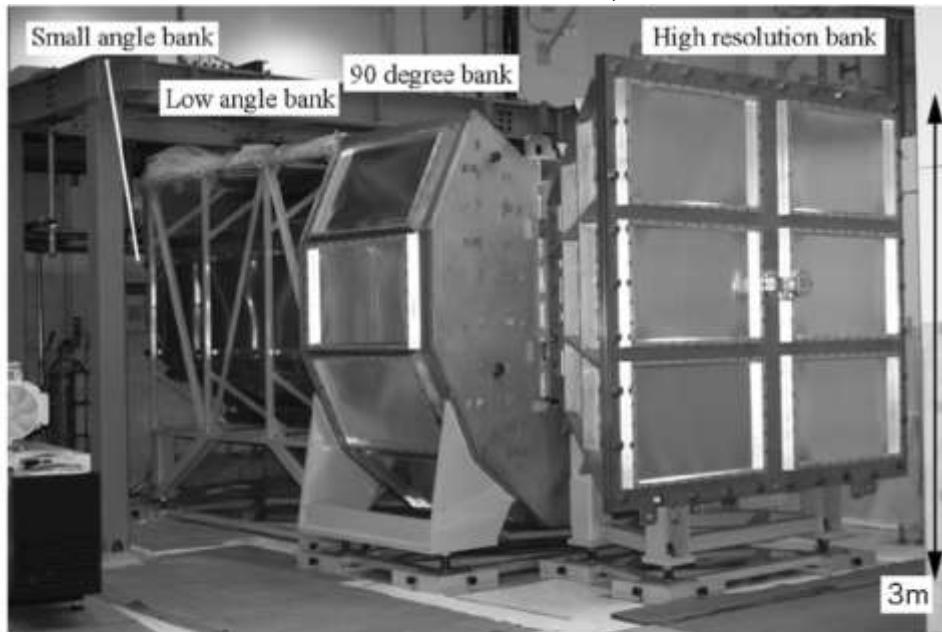
Fig. 2. IBARAKI Materials Design Diffractometer, iMATERIA without detector for each bank and instrument shieldings. High-resolution bank, special environment bank (90° bank), low angle bank, can be seen from right to left, and small angle detector bank, which are not shown in the picture, are situated in the low angle vacuum chamber (left hand of the picture).

SKAT data (micaceous quartzite)
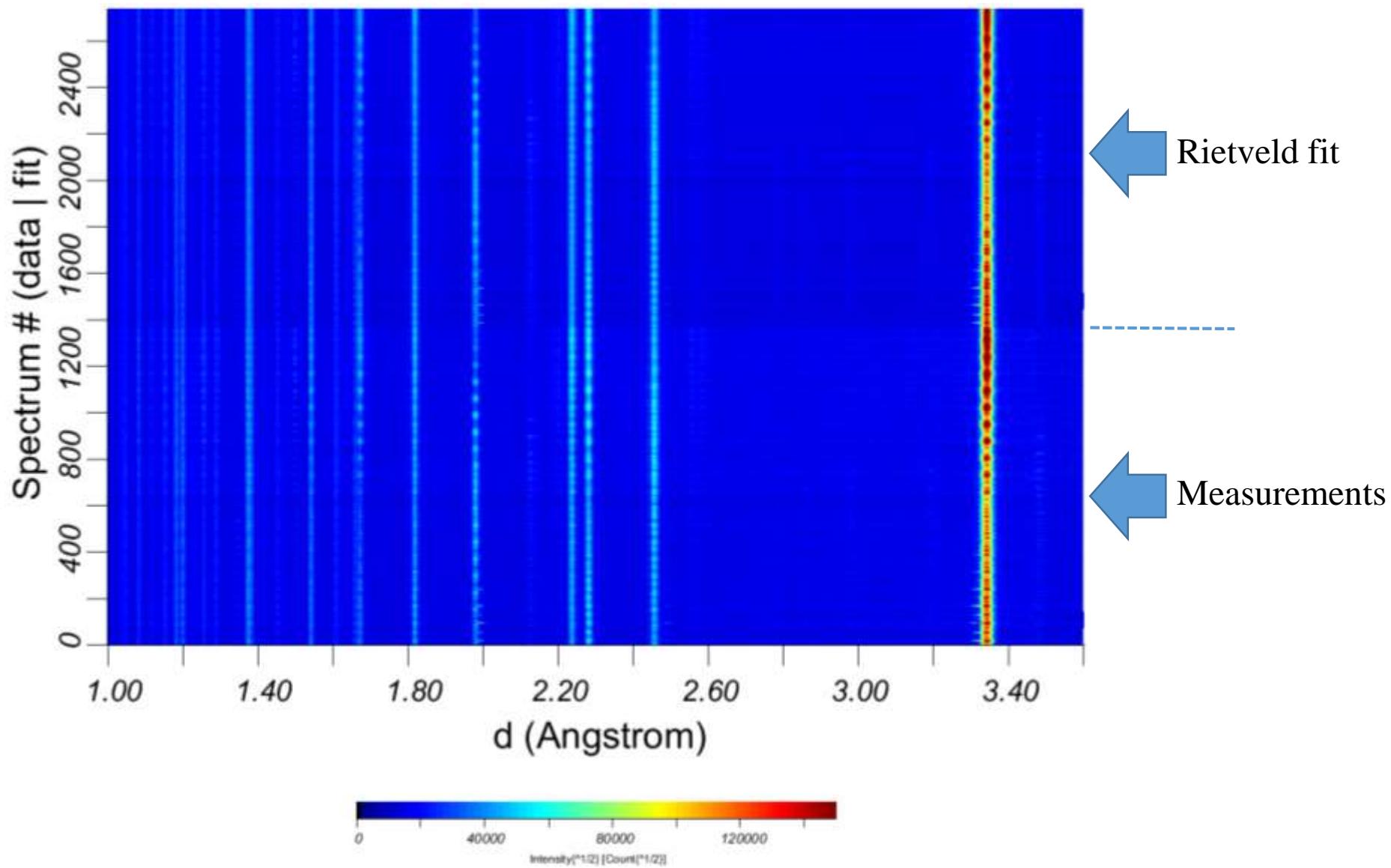
SKAT data (micaceous quartzite)

Dots = measurements, line = Rietveld fit

Foliation
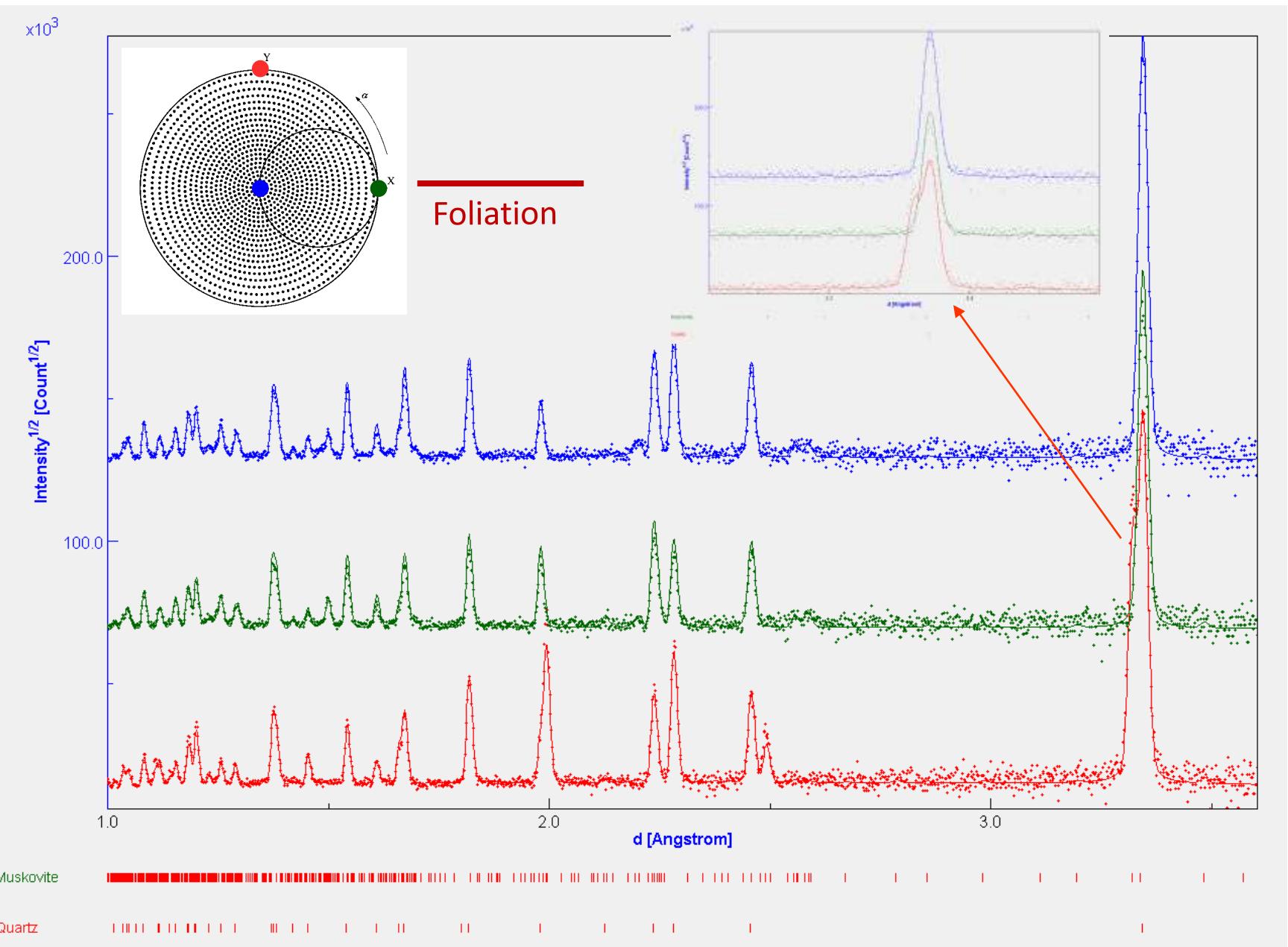
Properties of polycrystals: bulk elastic properties

What is required:

1. Properties of single-crystal (e.g., elastic tensor $^0C_{ijkl} \equiv \,^0S_{ijkl}^{\,-1}$)
2. ODF
3. Micromechanical model, that defines the averaging procedure

For single crystal: $\varepsilon = \,^0S\sigma; \quad \sigma = \,^0C\varepsilon$ Don't forget about indices! $\sigma_{ij} = \,^0C_{ijkl} \cdot \varepsilon_{kl}$

For polycrystal: $\bar{\varepsilon} = \bar{S}\bar{\sigma} = \overline{^0S\sigma}; \quad \bar{\sigma} = \bar{C}\bar{\varepsilon} = \overline{^0C\varepsilon}$ ⟶   Denotes some averaging procedure over all orientations

The simplest way to proceed is to assume that ε does not depend on orientation and apply arithmetic averaging over ODF; then $\overline{^0C} = \bar{C}$

$$\overline{C_{ijkl}} = \,^0C_{stuv} \int_G W_{is}(g)W_{jt}(g)W_{ku}(g)W_{lv}(g)\, f(g)\,dg$$

$W(g)$ is the orthogonal transformation matrix corresponding to rotation g,
$f(g)$ is ODF
The case of random ODF (=1) has been already reviewed 130 years ago…

Woldemar Voigt, 1887

Theoretische Studien

über die

Elasticitätsverhältnisse der Krystalle.

Von

W. Voigt.

Aus dem vierunddreißigsten Bande der Abhandlungen der königlichen Gesellschaft der Wissenschaften zu Göttingen.

Göttingen,
Dieterichsche Verlags-Buchhandlung.
1887.

Ξ-Axe indem wir über eine Kugelfläche integriren; der Nenner ist hier also $8\pi^2$. So erhält man:

$$(\alpha_1^2 \mathfrak{X}) = \frac{1}{8\pi^2} \int_0^\pi \int_0^{2\pi} \int_0^\pi d\varphi\, d\chi \sin^3\varphi \cos^2\chi (1 - \sin^2\varphi \cos^2\chi) \int_0^{2\pi} d\omega \cos^2 \omega = \frac{1}{15}$$

$$(\alpha_1^2 \mathfrak{Y}) = \frac{1}{8\pi^2} \int_0^\pi \int_0^{2\pi} \int_0^\pi d\varphi\, d\chi \sin^3\varphi \cos^2\chi (1 - \sin^2\varphi \sin^2\chi) \int_0^{2\pi} d\omega \cos^2(\varphi - \omega) = \frac{2}{15}$$

(64*)

$$(\alpha_1 \beta_1 \alpha_2 \beta_2) =$$

$$\frac{1}{8\pi^2} \int_0^\pi \int_0^{2\pi} \int_0^\pi d\varphi\, d\chi \sin^2\varphi \cos\chi \sin\chi \sqrt{1 - \sin^2\varphi \cos^2\chi} \sqrt{1 - \sin^2\varphi \sin^2\chi} \int_0^{2\pi} d\omega \cos\omega \cos(\varphi - \omega)$$

$$= -\frac{1}{30}$$

Setzt man kurz:

$$D_{11} + D_{22} + D_{33} = 3A, \quad D_{12} + D_{23} + D_{31} = 3B, \quad D_{44} + D_{55} + D_{66} = 3\Gamma,$$

so ergiebt sich hiernach aus (63):

$$(65) \quad \begin{aligned} A &= (\Delta_{11}) = \tfrac{1}{5}(3A + 2B + 4\Gamma), \\ B &= (\Delta_{12}) = \tfrac{1}{5}(A + 4B - 2\Gamma), \\ C &= (\Delta_{66}) = \tfrac{1}{5}(A - B + 3\Gamma). \end{aligned}$$

Hieraus folgt:

$$C = \frac{A - B}{2}$$

in Uebereinstimmung mit dem Resultate aller anderen Theorien; aber die anstössige Relation

$$A = 3B$$

ergiebt sich nur für den speciellen Werth $B = \Gamma$, der zwar, wie wir gesehen haben, nothwendig auftritt, wenn man Moleküle ohne Polarität voraussetzt, der aber durch die allgemeine Theorie nicht geliefert wird.

Durch die Annahme polarisirter Moleküle, welche aus vielen andern Gründen geboten erscheint, wird also der Widerspruch zwischen der molekularen Elasticitätstheorie und der Beobachtung vollständig gehoben.

Properties of polycrystals: bulk elastic properties

Micromechanical models:

- Voigt averaging (1887)
(arithmetic mean of C)

$$\bar{C}^{Voigt} = \overline{{}^0 C^A(g)^a}; \quad \varepsilon(g) = \bar{\varepsilon}$$

$$\bar{S}^{Reuss} \neq (\bar{C}^{Voigt})^{-1}$$

- Reuss averaging (1929)
(arithmetic mean of S)

$$\bar{S}^{Reuss} = \overline{{}^0 S^A(g)^a}; \quad \sigma(g) = \bar{\sigma}$$

- Hill (1952) & SuperHill (1995)

- GEO = geometric mean (1925-1965-1995)

$$(\bar{C}^{GEO})^{-1} = \bar{S}^{GEO} = \exp\left[\overline{ln\ {}^0 S^A(g)^a}\right]$$

- Self-consistent constructions (Eshelby 1957...) – stress field in ellipsoidal inclusion...

- SC+GEO = GeoMixSELF (Matthies 2010)

To be fulfilled:
1) $S = C^{-1}$
2) Group principle: for any division of a sample into a set of small volumes, the averaging over the whole volume of the sample is equivalent to the averaging of the averaged values of those small volumes

# Properties of polycrystals: bulk elastic properties

Simple model: isotropic polycrystal, only two different grain orientations are possible (denoted by blue and red colors).
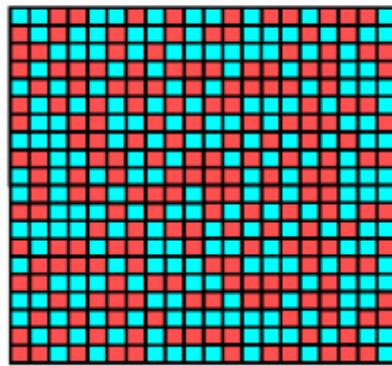

Equal strain
‘VOIGT’
delta L / L
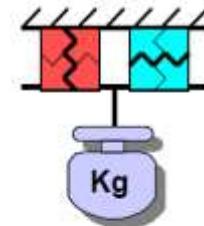
Equal stress
‘REUSS’
$s_1 = s_2$
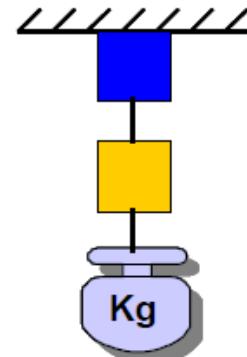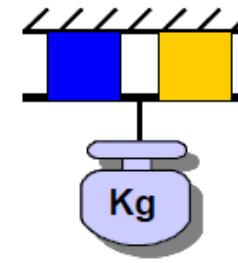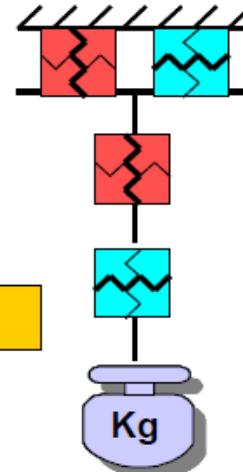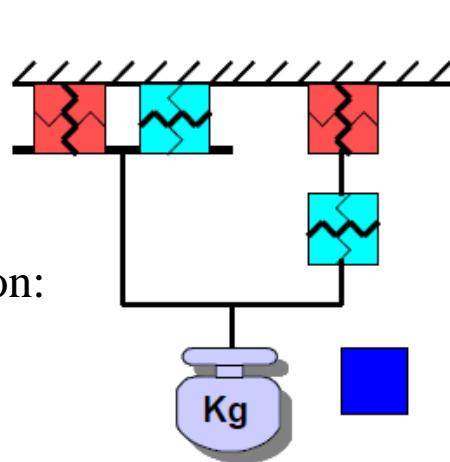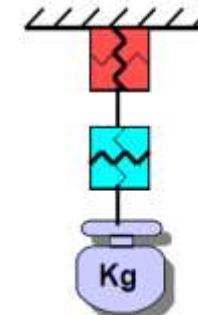
Hill's suggestion:

S. Matthies. On the combination of self-consistent and geometric mean elements for the calculation of the elastic properties of textured multi-phase samples. // Solid State Phenomena. 2010. V. 160. P. 87-93.

Properties of polycrystals: bulk elastic properties

Eshelby's procedure and its extensions.

There is an inclusion in a homogenous stress-free matrix C_{lqtv}.

1. Remove the inclusion and allow it to undergo the stress-free strain (*transformation*) ε^P_{tv} without altering its elastic constants.

2. Apply the surface traction $-\sigma^P_{lq}dS_l$ to the inclusion. This brings it back to the shape and size it had before transformation. Put it back in the matrix and reweld across S. The surface forces have now become a layer of body force spread over S.

3. Let these body forces relax, or, what comes to the same thing, apply a further distribution of $+\sigma^P_{lq}dS_l$ over S. The body is now free of external force but in a state of self-stress because of the transformation of the inclusion.

At this point, the total deformation of the inclusion is ε^G_{nw}.
The stress-free and total deformations are proportional:
$$\varepsilon^P_{tv} = T_{tvnw}\varepsilon^G_{nw}$$

Eshelby tensor, depends on ratios of elastic constants and axes of the ellipsoidal inclusion.

Eshelby: the strain and stress inside an ellipsoidal inclusion are uniform. Thus, T_{tvnw} could be solved (initially only the isotropic inclusion in an isotropic matrix has been considered, but soon it was extended for the case of general anisotropy).

*J.D. Eshelby. (1957) Proc. Roy. Soc. London A **241**, 376-396.*

Properties of polycrystals: bulk elastic properties

Eshelby's procedure and its extensions.

What if "matrix" elastic constants are not known, and all the inclusions are known? (How to assemble a polycrystalline body from single crystals of different phases with different orientations)?

It is possible to build an iteration procedure:

$$^{i+1}\mathsf{C} = {}^{i}\mathsf{C} + {}^{i}\mathsf{p} = {}^{i}\mathsf{C} + \overline{({}^{i}\mathsf{C} - {}^{i}\mathsf{E}^{-1}) \cdot {}^{i}\mathsf{u}}$$

$$^{i+1}\mathsf{S} = {}^{i}\mathsf{S} + {}^{i}\mathsf{q} = {}^{i}\mathsf{S} + \overline{{}^{i}\mathsf{u} \cdot {}^{i}\mathsf{S}}$$

$$^{i}\mathsf{u} = ({}^{0}\mathsf{C} - ({}^{i}\mathsf{C} - {}^{i}\mathsf{E}^{-1}))^{-1} \cdot {}^{i}\mathsf{E}^{-1} - \mathsf{I} \qquad {}^{i}\mathsf{E} = {}^{i}\mathsf{T} \cdot {}^{i}\mathsf{S}$$

$$I_{ijkl} = (\delta_{ik}\delta_{jl} + \delta_{il}\delta_{jk})/2$$

But p- and q-branches will only coincide for spherical grains!
To obtain a single solution (Geo-Mix-Self method):

$$^{i,GMS}\mathsf{C} \equiv {}^{i,GMS}\mathsf{S}^{-1} = SQRT^{SYM}({}^{i}\mathsf{C} \cdot {}^{i}\mathsf{S}^{-1}) = {}^{i}\mathsf{C}^{1/2} \cdot ({}^{i}\mathsf{C}^{-1/2} \cdot {}^{i}\mathsf{S}^{-1} \cdot {}^{i}\mathsf{C}^{-1/2})^{1/2} \cdot {}^{i}\mathsf{C}^{1/2}$$

E. Kröner (1958) Zeitschrift für Physik 151, 504-518.
S. Hirsekorn (1990) Textures and Microstructures 12, 1-14.
S. Matthies (2010) Solid State Phenomena 160, 87-93.
S. Matthies (2012) J. Appl. Crystallogr. 45, 1-16.

# Properties of polycrystals: bulk elastic properties

GEO-MIX-SELF

1. considers a macroscopic system with practically infinite (or at least very large) number of grains and thus is 'dimensionless', i.e. the ellipsoidal grain shape with axes $\{a_1, a_2, a_3\}$ is equivalent to $\{1, a_2/a_1, a_3/a_1\}$, etc.
2. takes no correlations between grain positions and orientations into account (as the ODF is not a correlation function).
3. allows no gaps or overlaps in the 'infinite' volume of the macroscopic material. This automatically leads to the conclusion that the GMS approximation virtually considers the distribution of the grains on size. For example, to fill the 3D volume with spheres without gaps, one has to assume a power law size distribution $\sim R^{-\alpha}$; R are the sphere's radii, α is close to 3 for the disordered packing [*T. Aste (1996) Phys. Rev. E* **53**, *2571-2579*].
4. allows for cracks/pores to be considered as inclusion with zero stiffness.

What is needed to "make" the elastic tensor of rock:
*   single crystal stiffness constants ^0C;
*   volume fractions of minerals and pores/cracks;
*   the ODFs of the minerals;
*   mass densities ρ that determine the density of the sample;
*   grain shapes and pores/cracks geometry approximated by ellipsoids;
*   shape orientation distribution functions $F(\Omega)$ for grains as well as for cracks and pores.

GMS averaging including grain shape: making shape ODF from ODF

a)

b)

1 mm

*H. Kern et al. (2008. Tectonophysics **457**, 143-149.*

We should consider the shape of biotite grains that are platelets (oblate spheroids).

X_E

Y_E
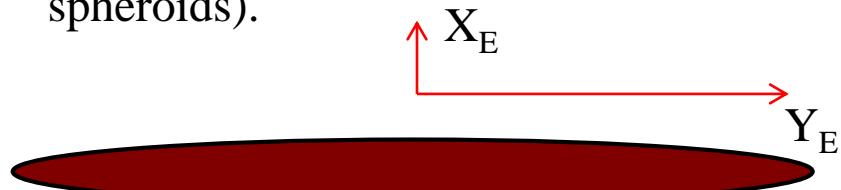
$X_E \approx$ min. Young's modulus
$Y_E \approx$ max. Young's modulus

X_B

Y_B

Fe
Mg
K
Si,Al
O
H
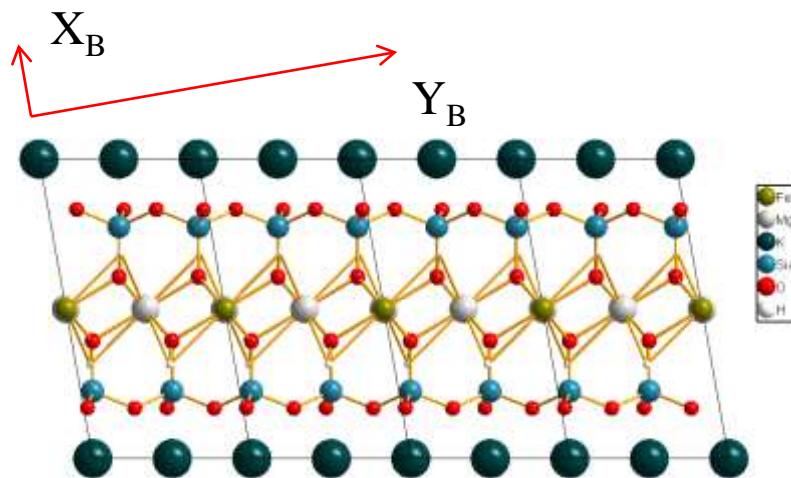
Relationship between crystal coordinate system K_B and grain coordinate system K_E should be taken into account when considering the grains shape and shape preferred orientation.

Tambo gneiss from Promontogno, Switzerland
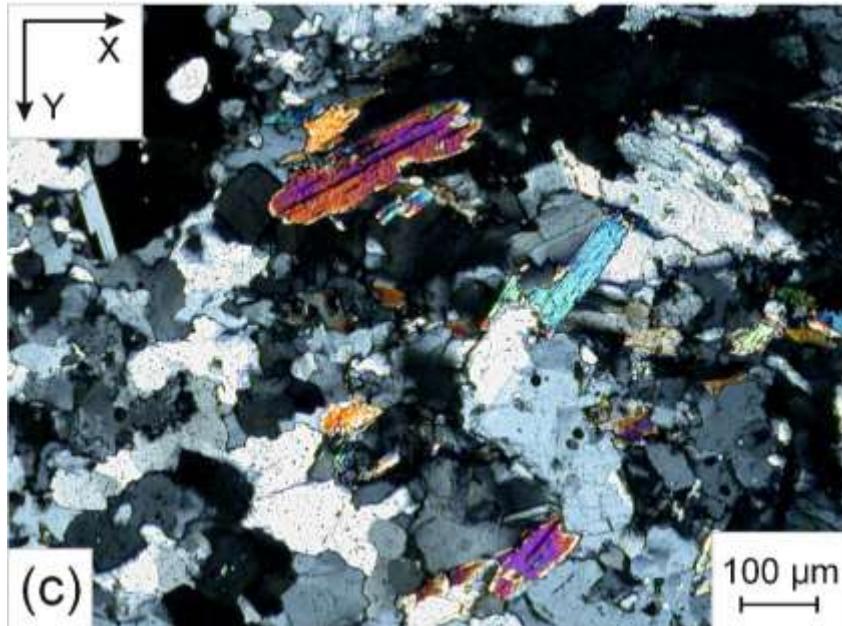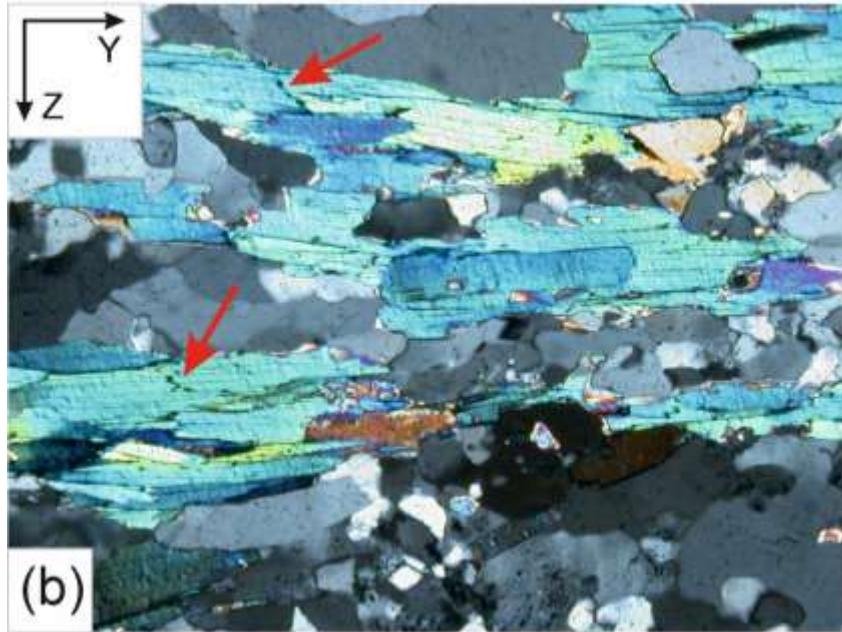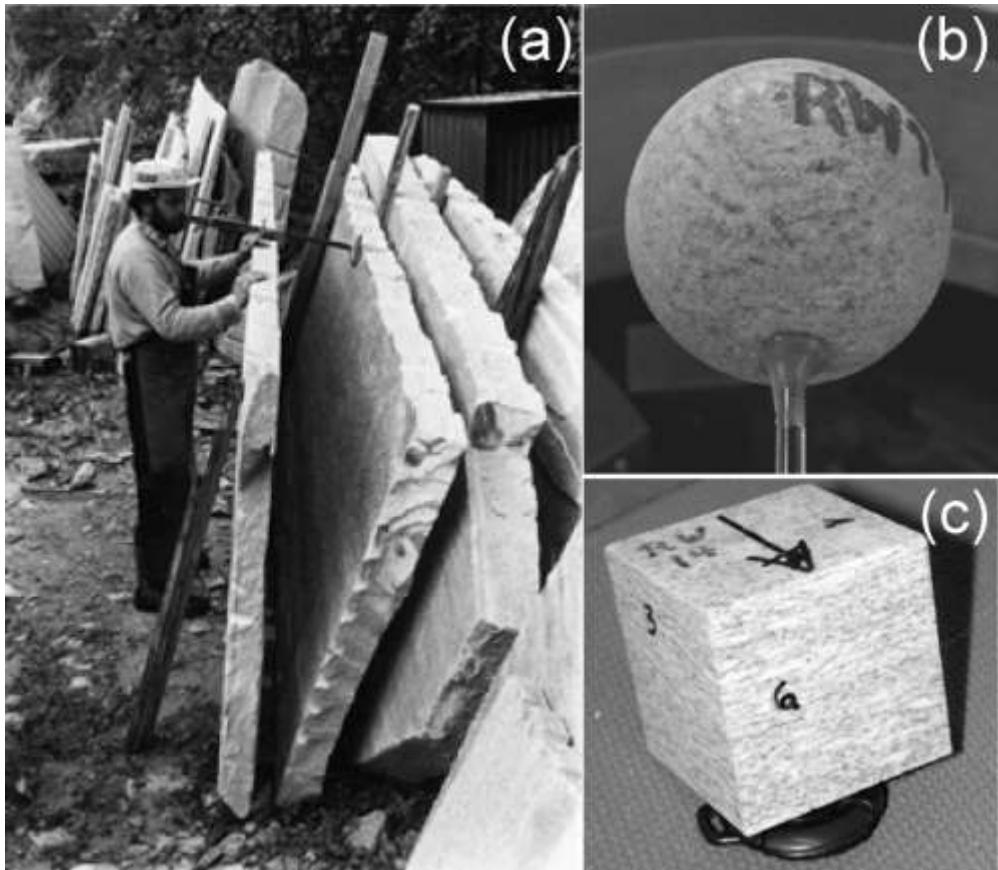
Tambo gneiss from Central Alps.
A particular property is that the rock easily cleaves into perfectly planar sheets that extend over meters and are used for large stone tables, roof plates and floors.

Tambo gneiss from Promontogno, Switzerland
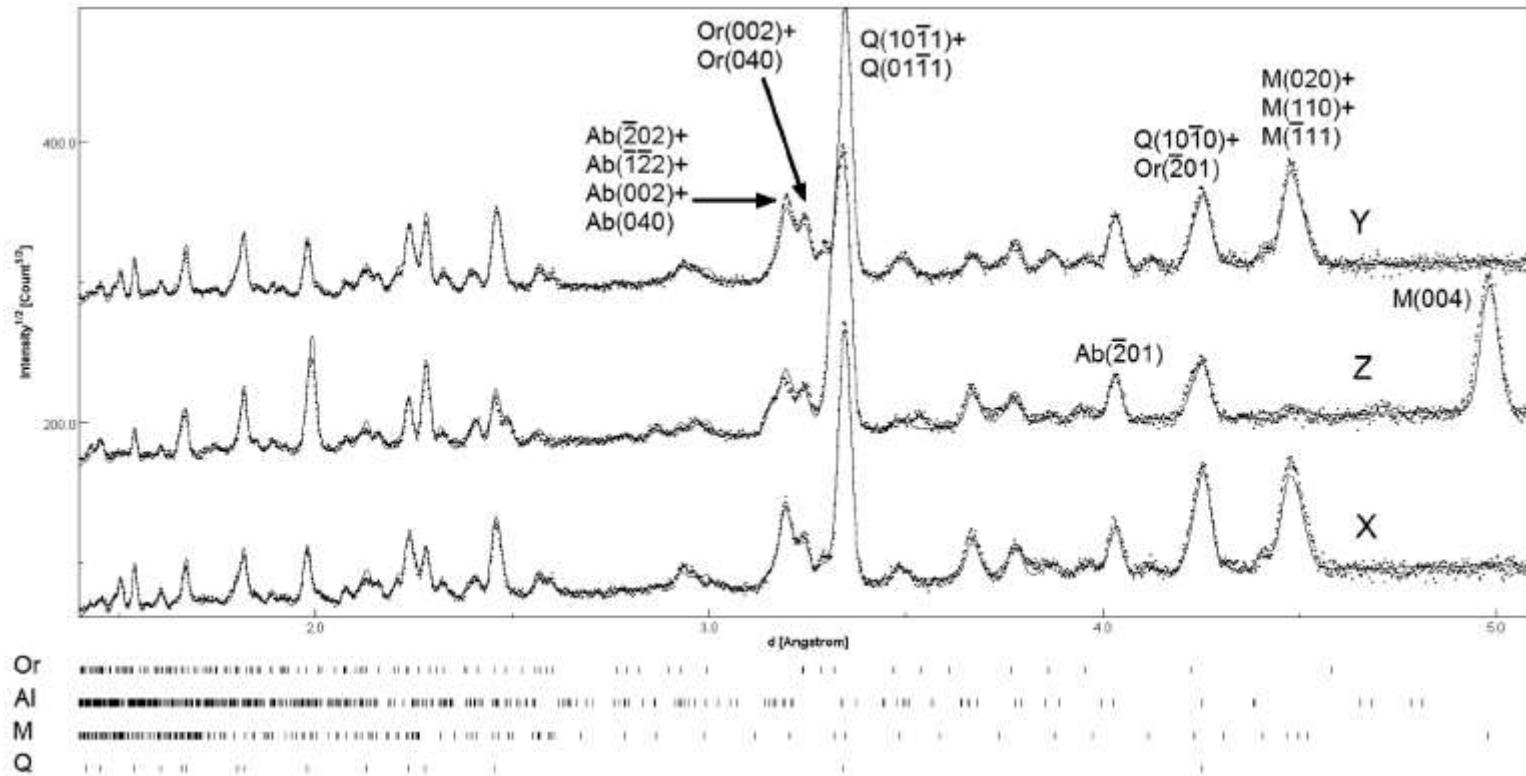
X – lineation (weak)

Z – foliation

Phase	Quartz	Albite	Orthoclase	Muscovite
Vol., %	38.7±2.6	25.8±1.7	18.0±1.2	17.5±1.2
ODF min.	0.24	0.06	0.32	0.04
ODF max.	3.10	13.22	2.61	16.53
F2	1.19	1.27	1.09	3.58

Tambo gneiss from Promontogno, Switzerland

(a)   (b)   (c)

Long axis

Short axis
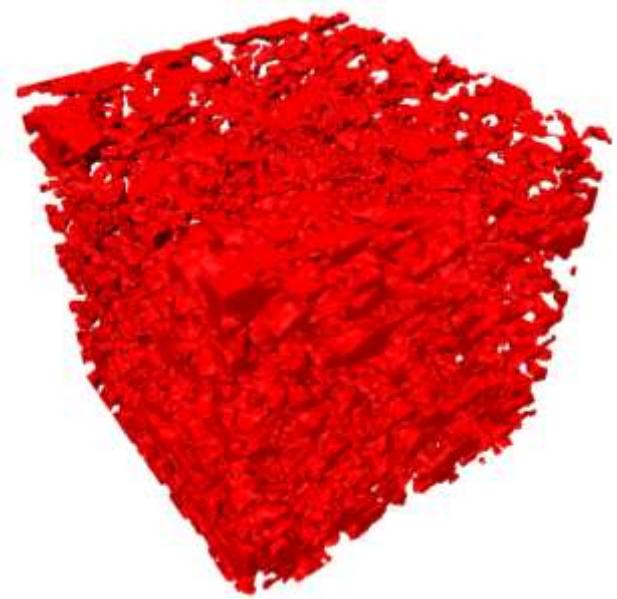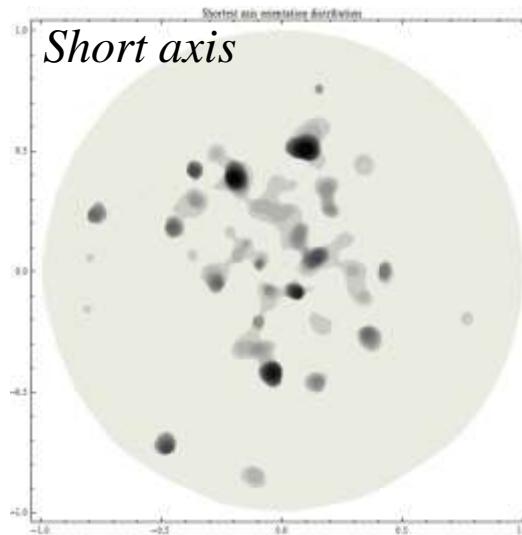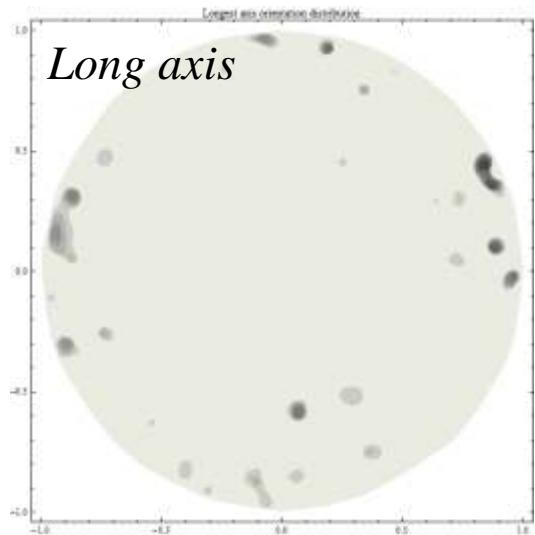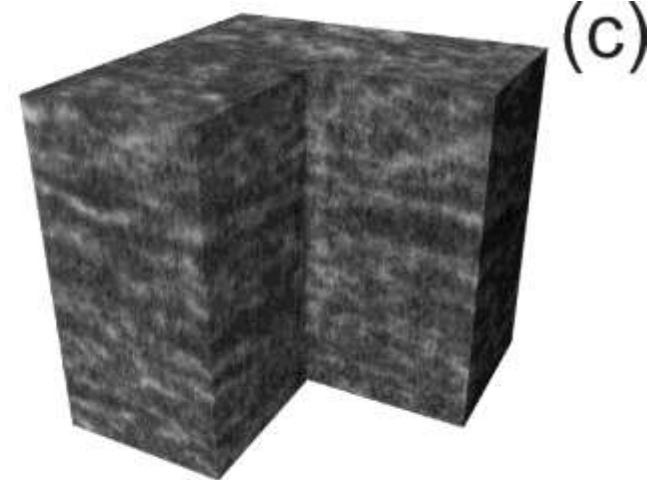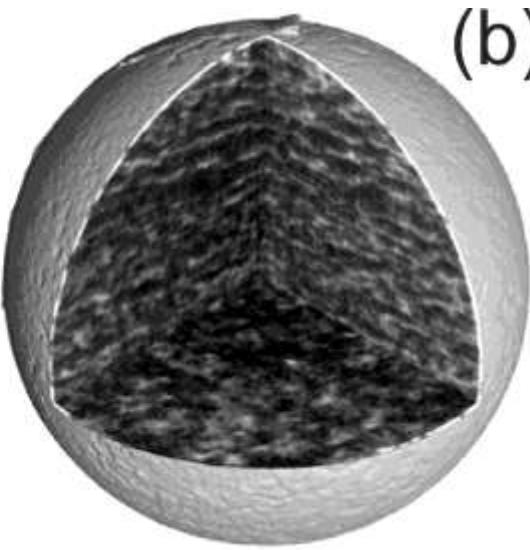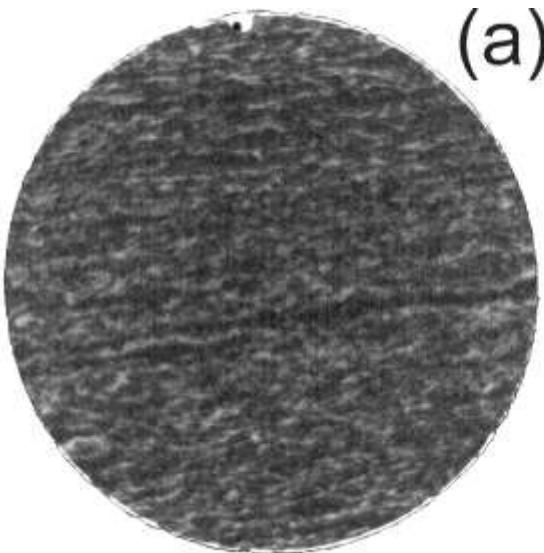
Framework of mica grains in the gneiss and their shape preferred orientations

Tambo gneiss from Promontogno, Switzerland
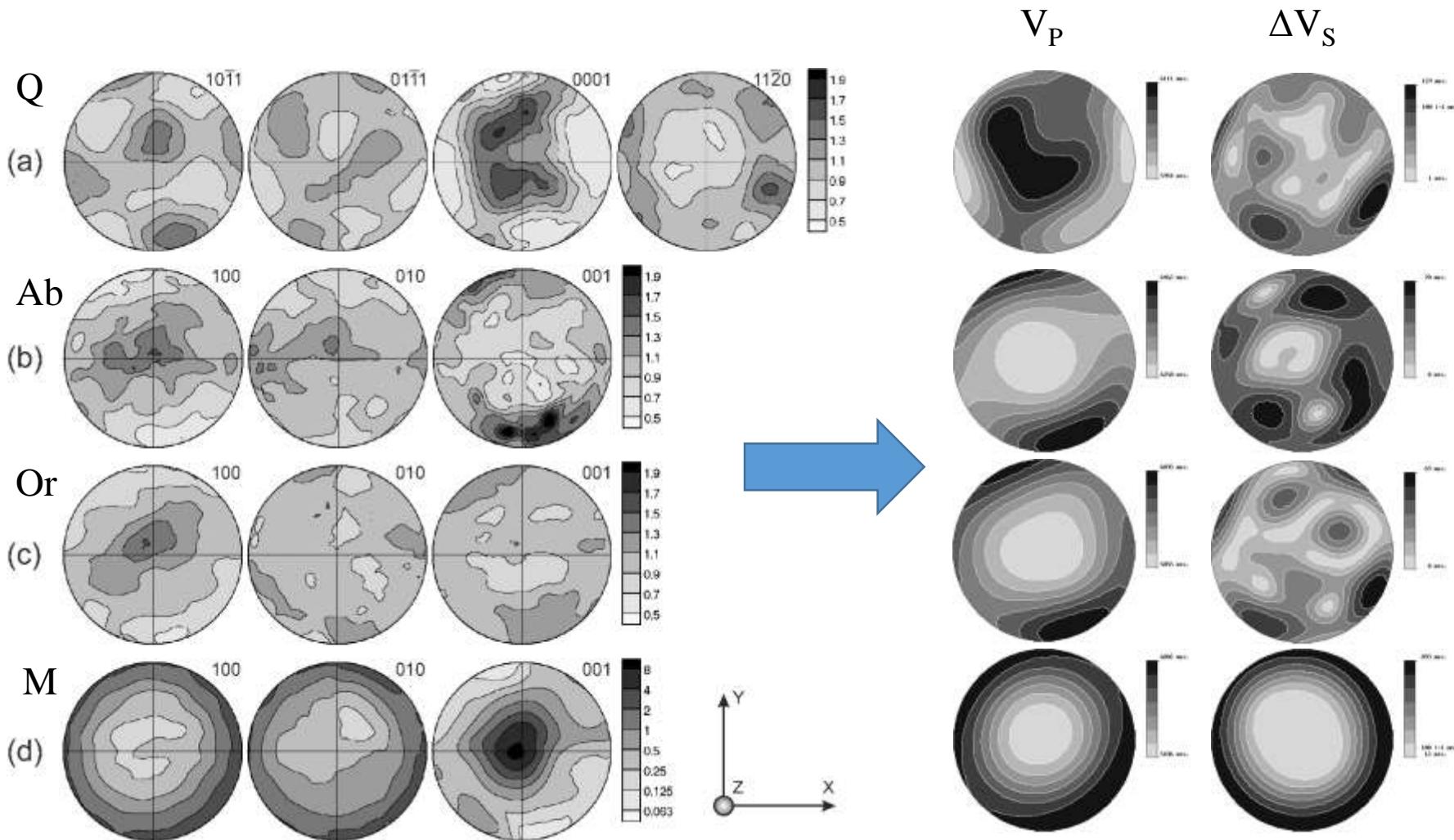
Texture-based recalculation of elastic wave velocities for different minerals

Ultrasonic experiments on spherical samples

Institute of Geology, Academy of Sciences of Czech Republic, Prague

Measuring head in high pressure chamber. Sample diameter is 5 cm (same as the sample size for th SKAT diffractometer). Two resonant longitudinal wave transducers, 2 MHz, can be used up to 400 MPa; pairs of shear wave transducers, 0.8 MHz, can be used up to 100 MPa.

T. Lokajíček and T. Svitek (2015) Ultrasonics, DOI: 10.1016/j.ultras.2014.08.015

Velocity measurement grid, 15° steps, 132 directions
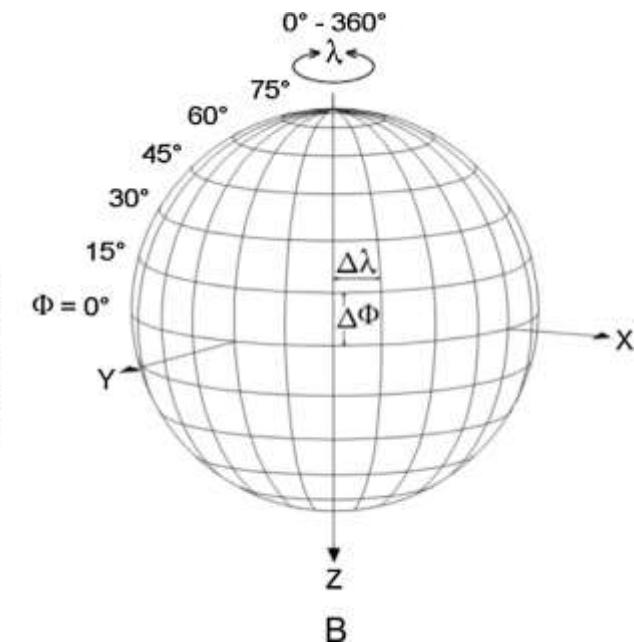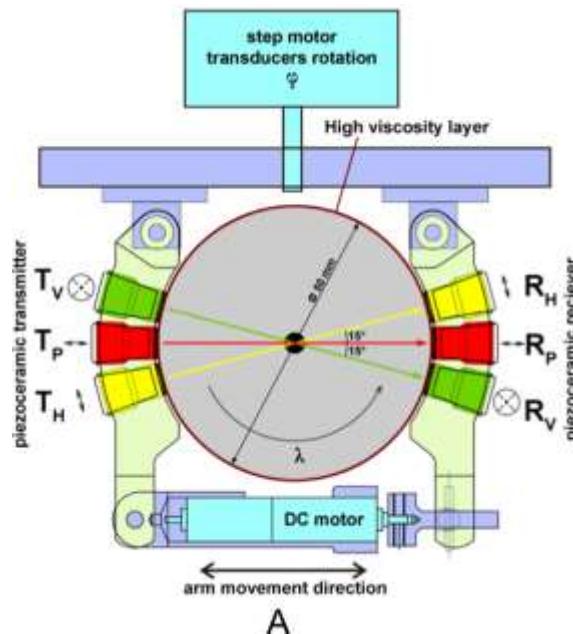
How to compare measured velocities and model C_{ijkl}'s?

1. Recalculate wave velocities from C_{ijkl} set → often large sets of velocities are available (> than number of independent elastic constants), and numerical comparison is troublesome.

2. Recalculate C_{ijkl} from measured velocities → complicated, not always possible with only one type of waves (e.g., only P-waves & isotropic or transversely isotropic or hexagonal symmetry).

Either way, we need a relation C_{ijkl} ↔ measured velocities.

Common approach:

Flat wave:
$$\boldsymbol{u} = A\boldsymbol{p}\, exp[\tfrac{2\pi i}{\lambda}(\boldsymbol{n}\cdot\boldsymbol{r} - Vt)];$$

For displacements in the elastic field: $\qquad C_{ijkl}\dfrac{\partial^2 u_l}{\partial x_j \partial x_k} = \rho\dfrac{\partial^2 u_i}{\partial t^2}:$

Christoffel equation: $\quad C_{ijkl}n_i n_k p_l = M_{il}p_l = \rho V^2 p_i \qquad$ Eigenvalues problem.

Things to remember: Christoffel equation is for a flat wave. Thus wavelength of the elastic wave should be << size of the sample.

Phase velocity with eigenvector of Christoffel tensor M (that is the polarization vector **p**) closest to propagation direction **n** is V_P; it is not necessary the fastest velocity in anisotropic material!

Fastest of two remaining waves is V_{S1}, slowest is V_{S2}.

It is tricky to construct the refinement of C_{ijkl} from measured velocities of strongly anisotropic material because of this 'ordering' part!
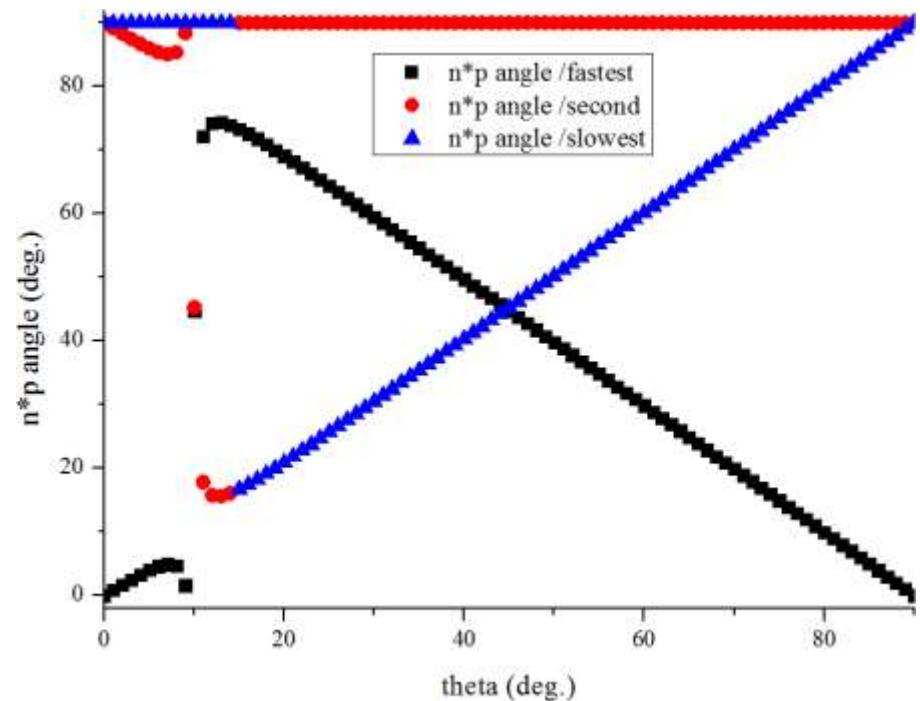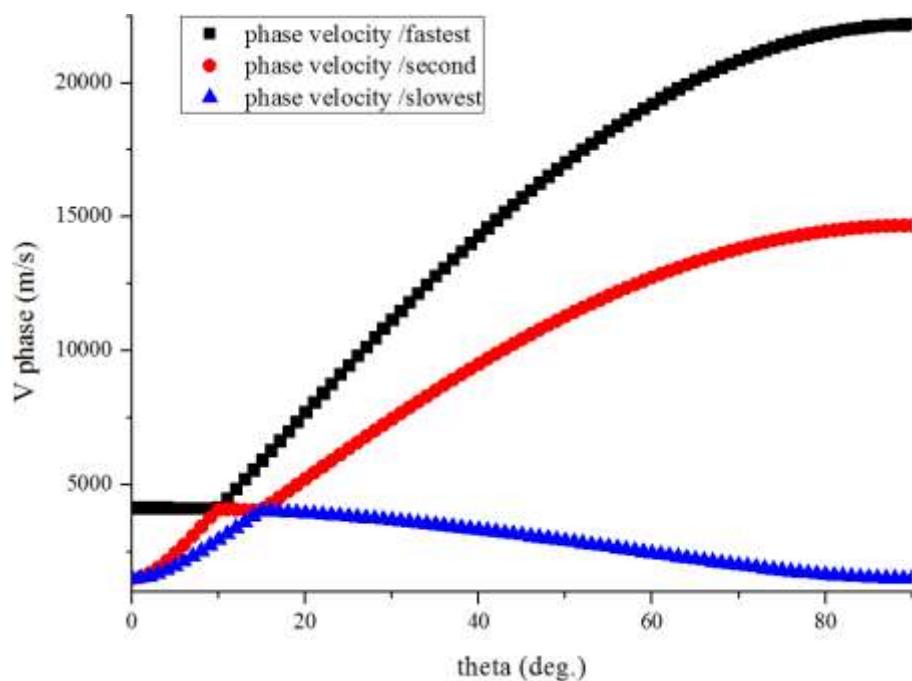
Graphite single crystal (hexagonal symmetry)
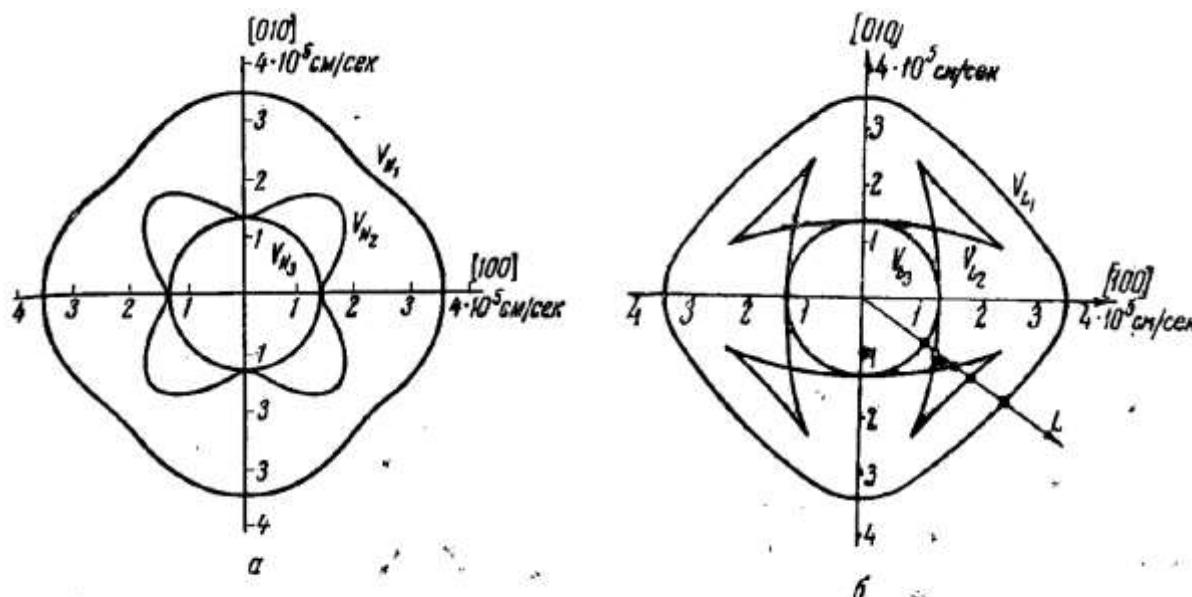
Рис. 1. Сечения поверхности нормальных скоростей *a* и волновой поверхности *b* кубического кристалла KBr плоскостью симметрии (001).

K.S. Aleksandrov (1958) The wave surfaces for elastic waves in crystals. Kristallografiya (Crystallography Reports) 3, 620-623.
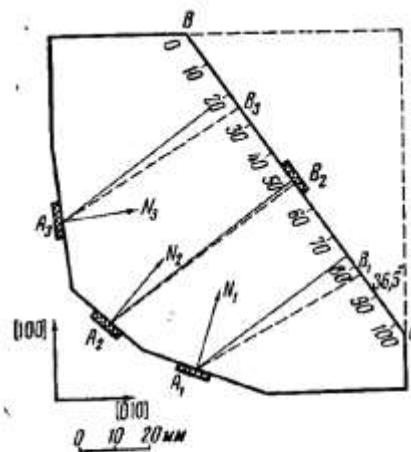

Рис. 3

Рис. 3. Ориентировка образца по данным рис. 2.

Рис. 4

Рис. 4. Экспериментальная зависимость энергии принятого сигнала от положения приемника на грани *BC* образца.

B_1, B_2, B_3 — положения максимумов энергии принятого сигнала при помещении излучающей пластинки соответственно на гранях A_1, A_2, A_3.
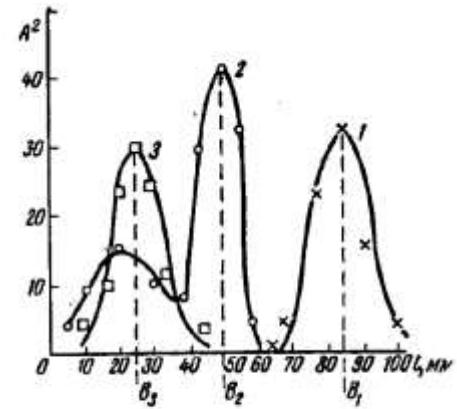
Group velocity?

$$W = \frac{\partial \omega}{\partial k}$$

Using Christoffel equation solutions, e.g., $W_j\big|_P = \frac{1}{\rho V_P} C_{ijkl} \cdot p_i\big|_P \cdot p_k\big|_P \cdot n_l$ (and + similar 2 for S-waves)

Situation is more complicated in this case!

Different waves propagating in different directions could be detected by the same single sensor (in some cases, for 1 ray direction there are up to 5 different waves).
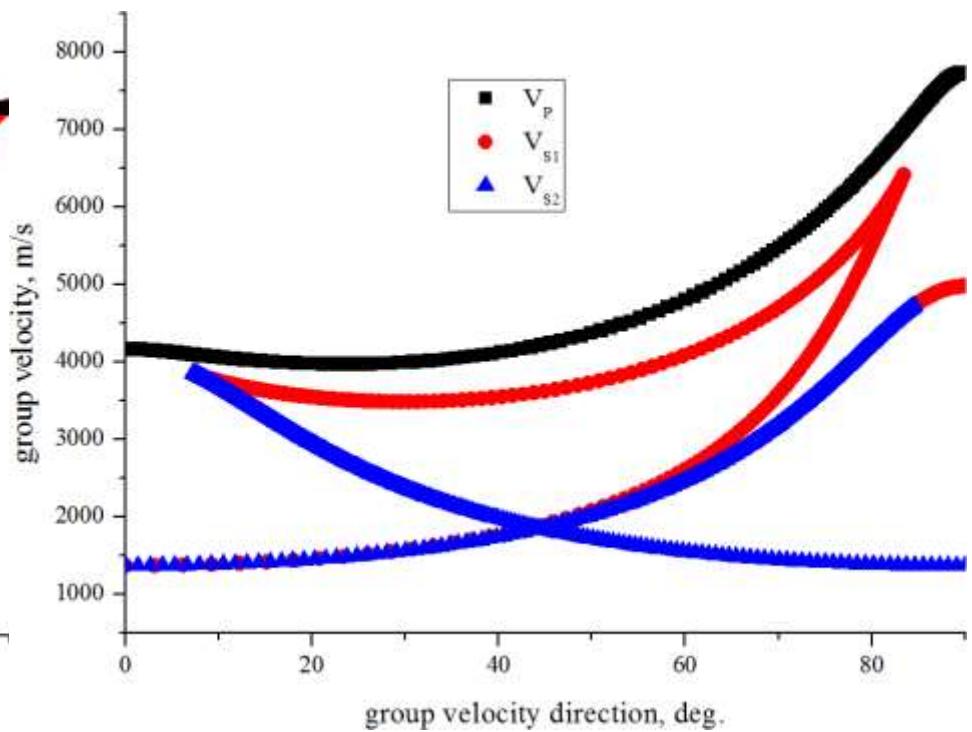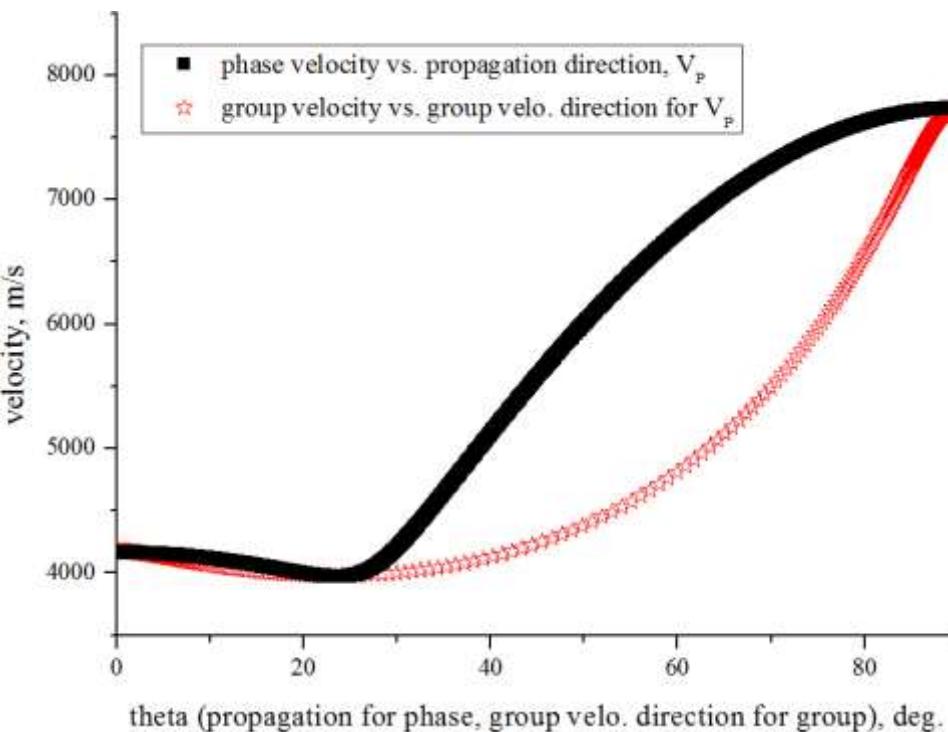
Biotite single crystal (quasi-hexagonal symmetry!

But if phase and group velocities are plotted against the wave front normal direction, group velocities always should be greater (or equal) because phase velocity is group velocities' projection onto the wave front normal.
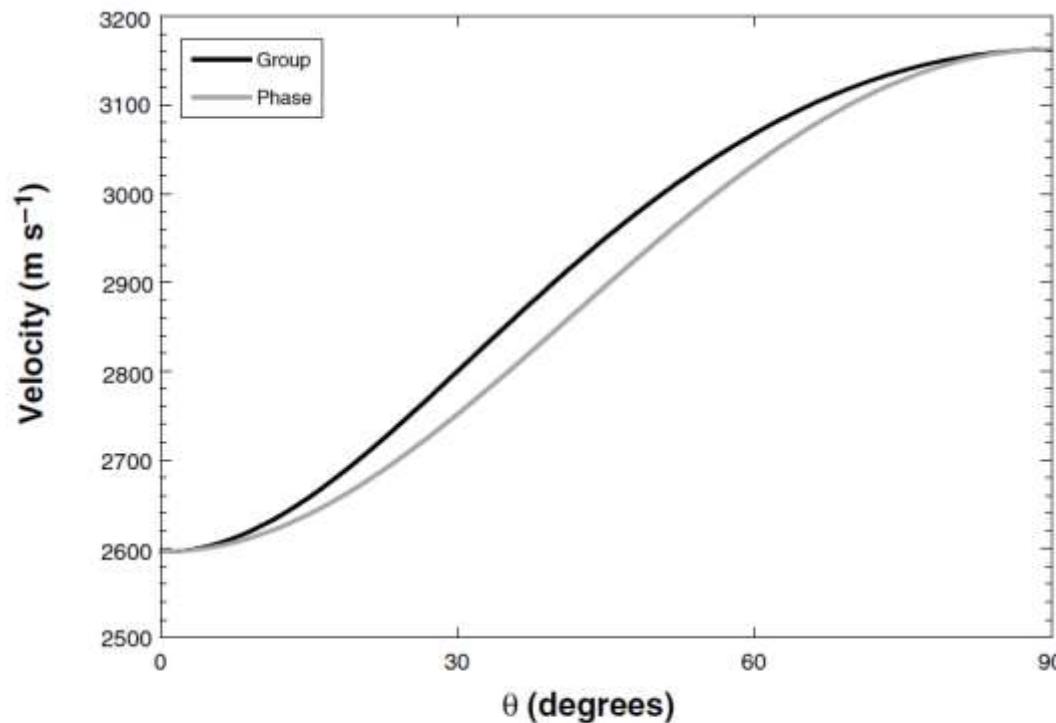
**Figure 5.** Group and phase velocity surfaces for the Muderong Shale at one effective stress condition.

D.N. Dewhurst, A.F. Siggins. (2006)
Geophys. J. Int. **165**, 135-148.

Things to remember: model 'averaged' C_{ijkl} represent 'effective medium' properties, thus they will work if wavelength of elastic wave is >> size of heterogeneities in material.

This condition depends on the "contrast" of elastic properties and proportions of materials.

If elastic constants are about the same, ">" is practically sufficient.

K. Helbig (1984) Geophysics **49**, 364-373.
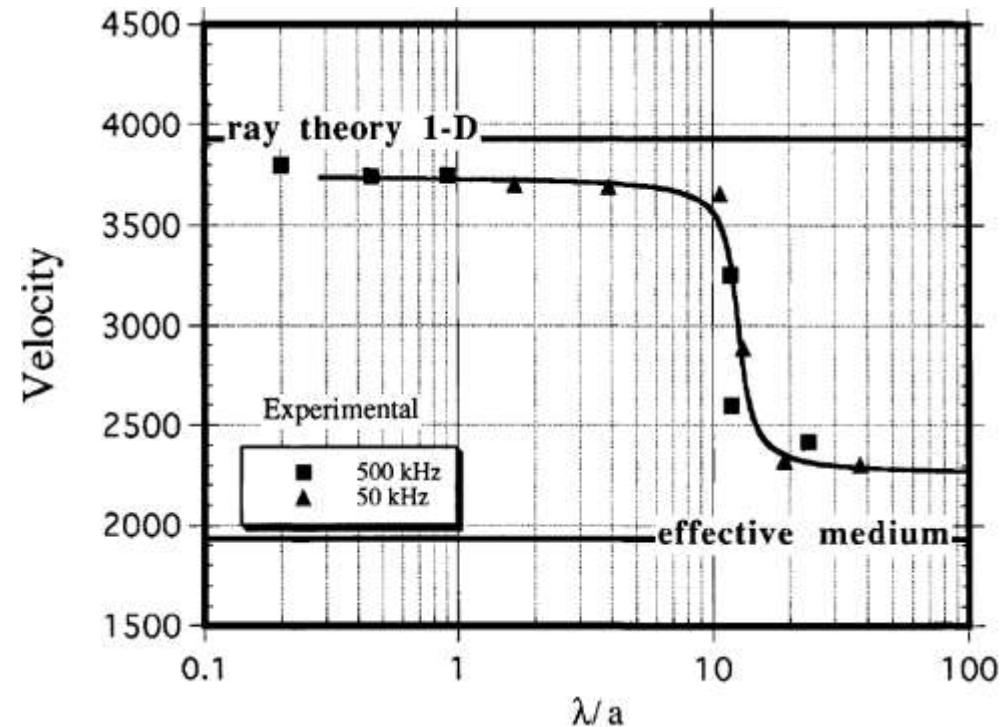
Elastic wave velocity in stratified steel-plastic composite.

T. Mukerji et al. (1995)Geophysics **60**, 1222-1233.

Extra complication

If we are particularly unlucky to have quartz, we have to account for the spacial dispersion
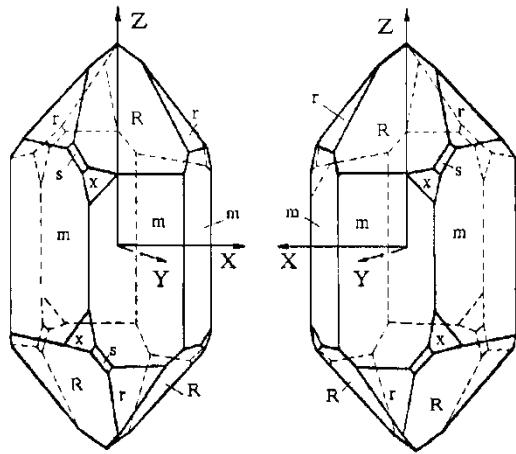
Left-handed quartz structure:

P3$_2$21 (№154)

Si: 3a (x, 0, 2/3);

O: 6c (x, y, z)

Right-handed quartz structure:

P3$_1$21 (№152)

Si: 3a (x, 0, 1/3);

O: 6c (x, y, z)

$$C_{ijkl} \frac{\partial^2 u_l}{\partial x_j \partial x_k} + b_{ijkln} \frac{\partial^3 u_l}{\partial x_j \partial x_n \partial x_k} = \rho \frac{\partial^2 u_i}{\partial t^2}:$$

b – acoustic gyration tensor

$$(M_{jk} + i\delta_{jkl}Q_l)p_k = \rho V^2 p_j \qquad Q_s = \frac{\pi}{\lambda}\delta_{sjk}b_{ijkln}n_i n_l n_n$$

In quartz for **n**‖3-fold axis and $\omega \approx 3$ MHz rotation of the polarization plane is $\approx 10°$/cm, while relative correction for the velocity values is less then 10^2.

And we need to know whether there is left or right quartz in the material, or their ratio and orientation distributions for each of them

# Tambo gneiss from Promontogno, Switzerland

Measured, 0.1 MPa (a)
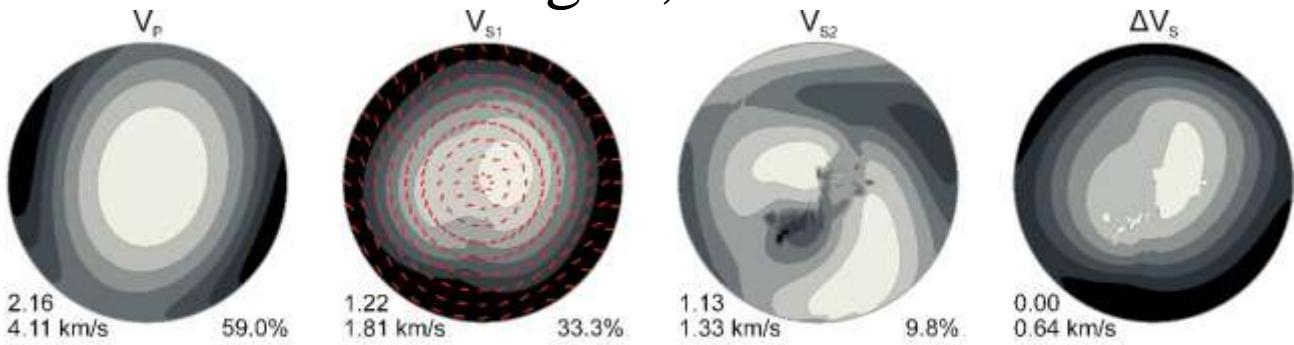
Measured, 100 MPa (b)
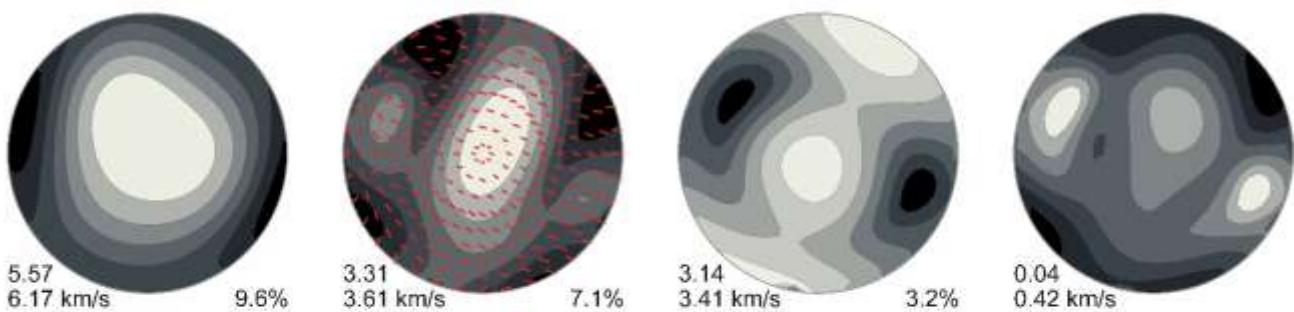
Model, no cracks (c)
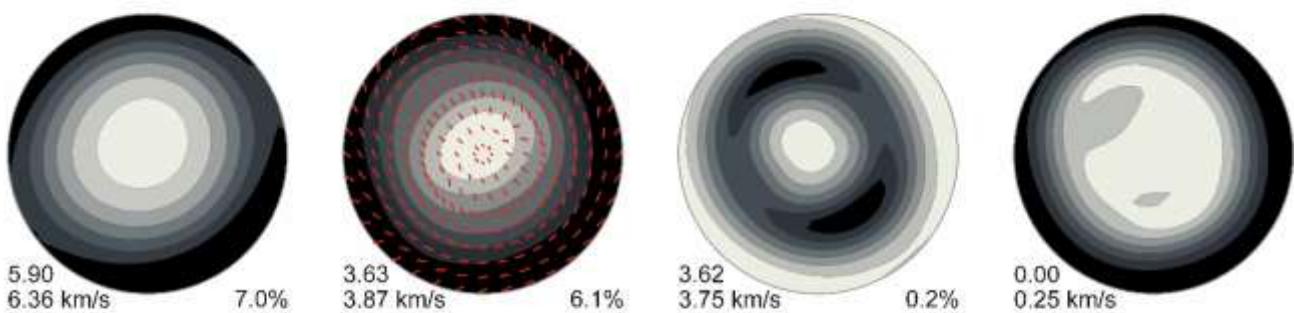
Model, 0.1 Vol.% of (d)
cracks || mica

V_P V_{S1} V_{S2} ΔV_S

(a)
2.16 / 4.11 km/s — 59.0%
1.22 / 1.81 km/s — 33.3%
1.13 / 1.33 km/s — 9.8%
0.00 / 0.64 km/s

(b)
5.57 / 6.17 km/s — 9.6%
3.31 / 3.61 km/s — 7.1%
3.14 / 3.41 km/s — 3.2%
0.04 / 0.42 km/s

(c)
5.90 / 6.36 km/s — 7.0%
3.63 / 3.87 km/s — 6.1%
3.62 / 3.75 km/s — 0.2%
0.00 / 0.25 km/s

(d)
5.63 / 6.28 km/s — 10.0%
3.56 / 3.84 km/s — 7.3%
3.54 / 3.67 km/s — 0.3%
0.00 / 0.30 km/s
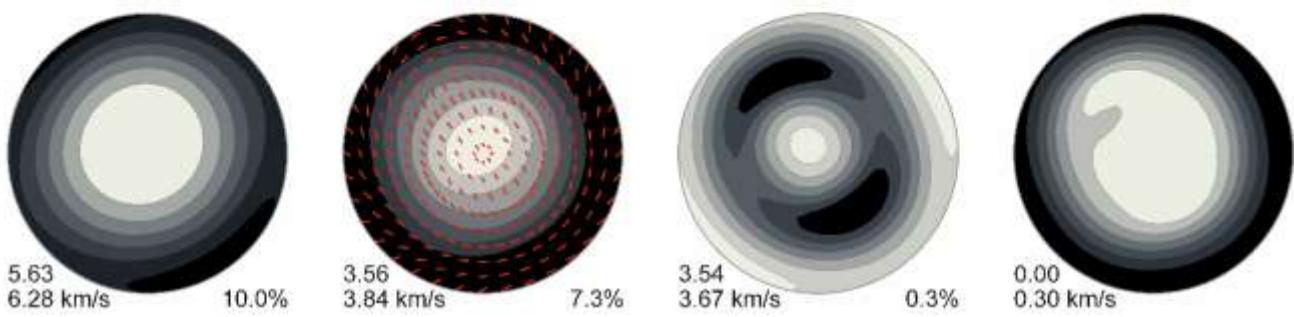
Tambo gneiss from Promontogno, Switzerland

Measured, 100 MPa
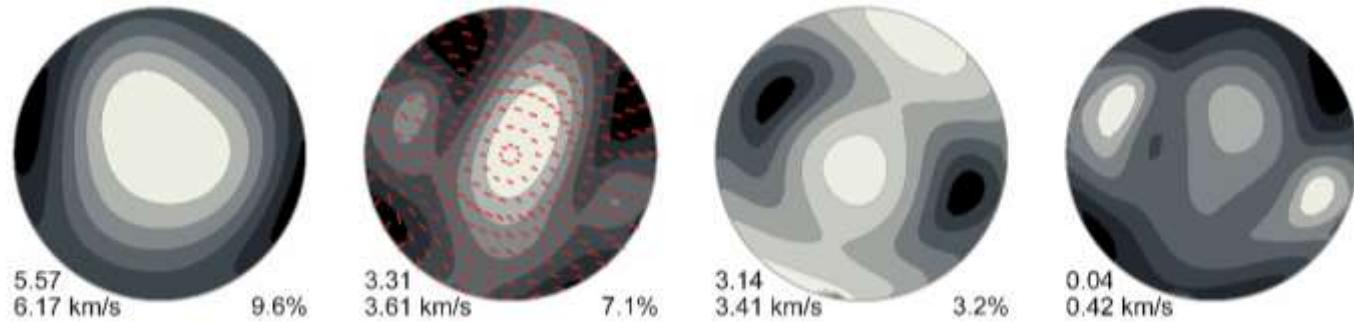
Model, with 0.1 Vol.% cracks ‖ mica and 0.6 Vol.% of secondary cracks (normal to mica grains and ‖ lineation)
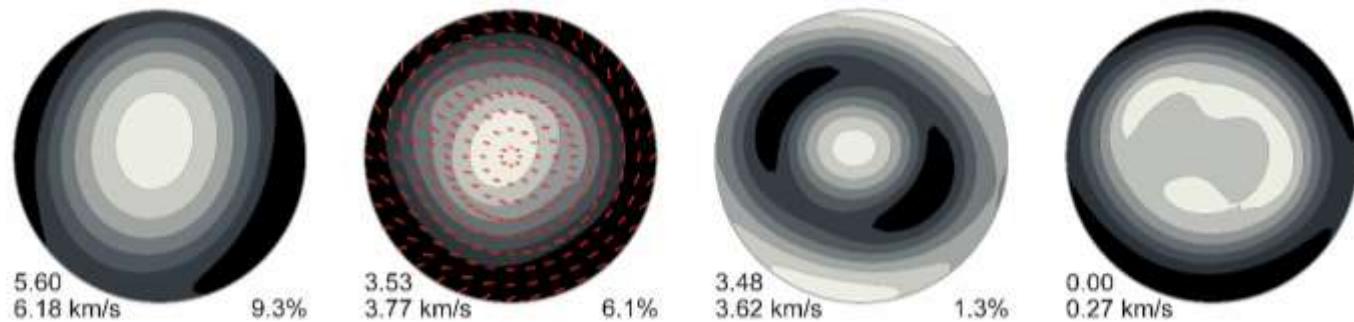
Not a very good agreement of a room pressure measurements with a model (probably, due to lots of cracks produced by blasting, which makes measurements and modelling significantly more complicated)

Anisotropy coefficient:
$A\text{-}V_P[\%] = 100\% \cdot (V_{Pmax} - V_{Pmin})/V_{Pmean}$

Tambo gneiss from Promontogno, Switzerland

Table 5. Bulk elastic properties of Tambo gneiss calculated from ultrasonic measurements (second run, with both P and S velocities) on the spherical sample, as well as elastic constants of two Tambo gneiss models including crack systems (all values are in GPa).

|	Inverted from measurements at 100 MPa	Model: 0.1 vol.% of primary cracks and 0.6 vol.% of secondary cracks	Inverted from measurements at 0.1 MPa	Model: 2.6 vol.% of primary cracks and 1.0 vol.% of secondary cracks
C_{11}	99.2	99.8	42.9	43.8
C_{12}	30.3	23.1	17.0	5.9
C_{13}	27.8	21.9	15.0	2.9
C_{14}	− 1.4	− 0.1	− 0.5	− 0.4
C_{15}	− 1.5	0.9	− 1.4	1.6
C_{16}	− 1.7	− 0.8	− 2.8	− 2.1
C_{22}	93.8	95.6	26.8	40.3
C_{23}	32.3	21.0	9.7	2.9
C_{24}	− 0.9	− 1.2	− 0.8	− 1.9
C_{25}	1.0	0.1	− 0.6	0.3
C_{26}	0.4	− 0.6	− 2.5	− 2.0
C_{33}	82.2	82.7	12.3	13.1
C_{34}	− 0.7	− 0.5	− 0.1	− 1.0
C_{35}	− 0.1	0.3	− 0.5	0.8
C_{36}	3.6	0.0	− 1.9	− 0.2
C_{44}	26.4	32.1	3.6	9.7
C_{45}	− 1.0	− 0.2	0.2	− 0.5
C_{46}	0.5	0.3	0.2	0.7
C_{55}	28.6	32.9	4.3	10.1
C_{56}	0.6	− 0.4	− 0.4	− 0.9
C_{66}	32.6	37.2	8.5	18.1

Micaceous quartzite

A muscovite-bearing quartzite sample from the TRANSALP seismic traverse (Eastern Alps, Austria)

11.9 Vol.%, F2=12.0

A small amount of pores and cracks is present in the rock; now we can include them into models of bulk physical properties

88.1 Vol.%, F2=1.4

*R.N. Vasin et al. (2014) ICOTOM-17, Book of Abstracts, Dresden, Germany, 2014. P. 182.*
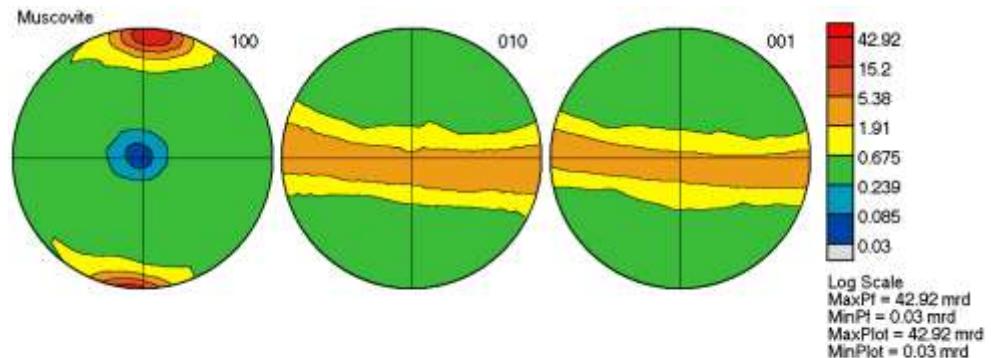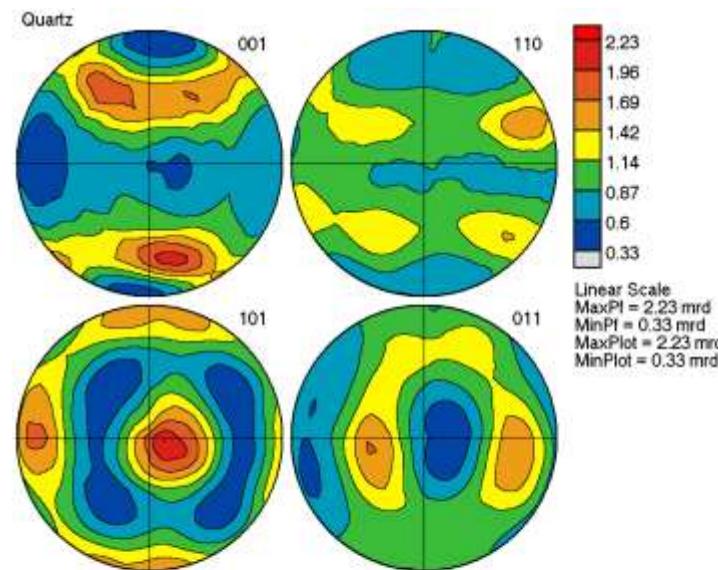
Results of ultrasonic measurements – anisotropy changes due to pores

*0 MPa*

1936 m/s
5817 m/s (100.1%)

10 MPa

2894 m/s
6005 m/s (69.9%)

20 MPa
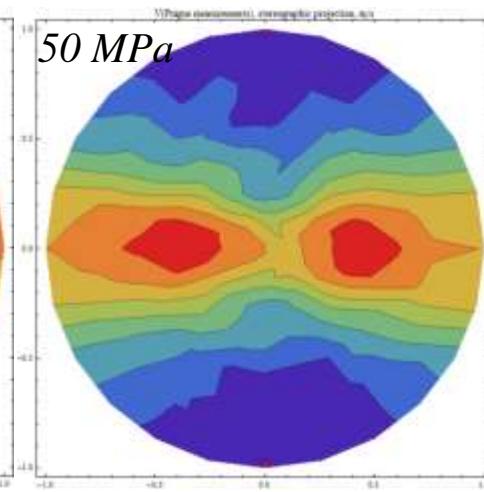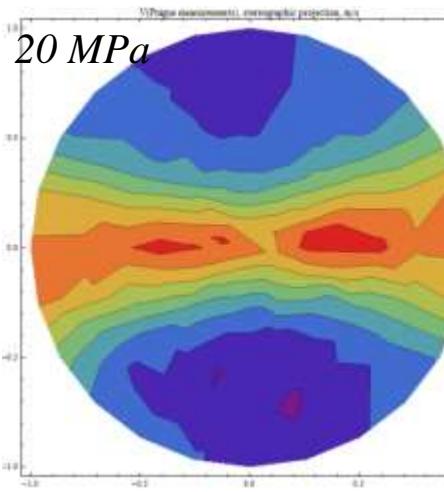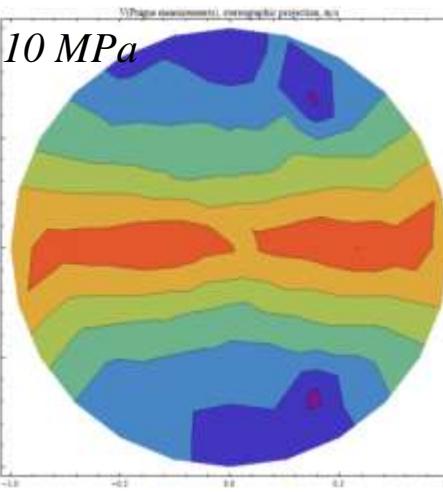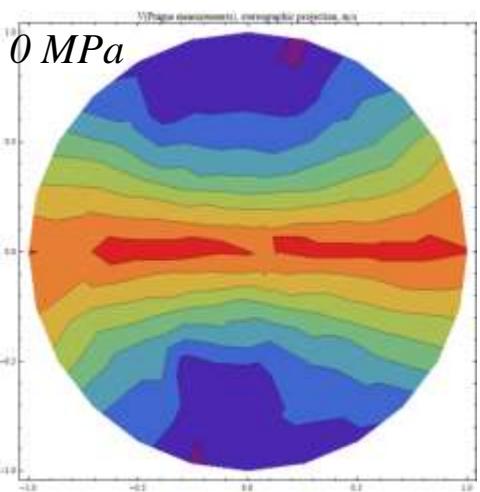
4372 m/s
5892 m/s (29.6%)

50 MPa

5384 m/s
6168 m/s (13.6%)

Foliation

100 MPa

5614 m/s
6261 m/s (10.9%)

200 MPa

5740 m/s
6340 m/s (9.9%)

300 MPa

5652 m/s
6207 m/s (9.4%)

400 MPa
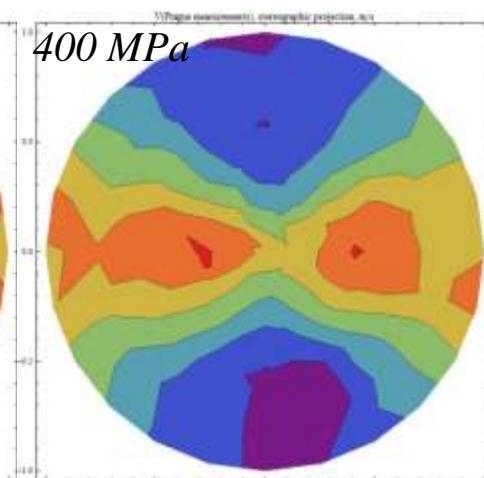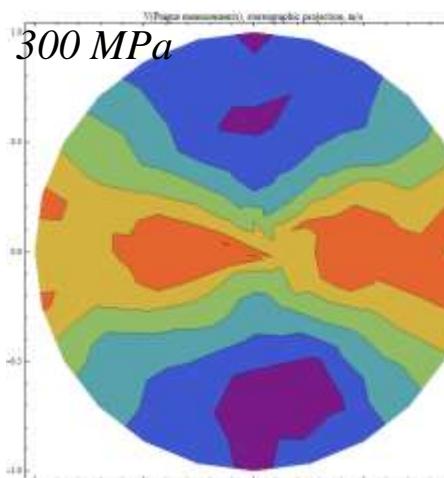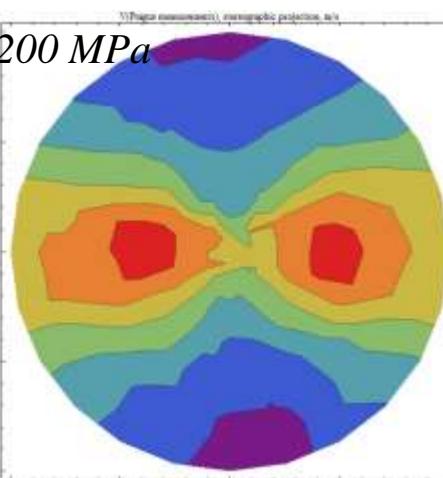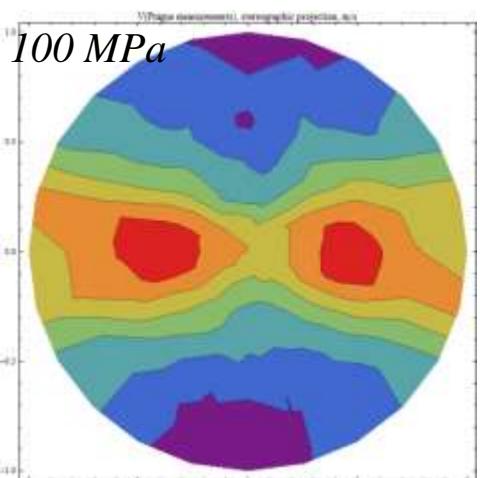
5756 m/s
6316 m/s (9.3%)

Stereographic projections, linear scale contours, $k_P = 200\% * (V_{Pmax} - V_{Pmin})/(V_{Pmax} + V_{Pmin})$

Adding pores at higher pressures…


Model with 0.08 Vol%
of pores || to
muscovite grains
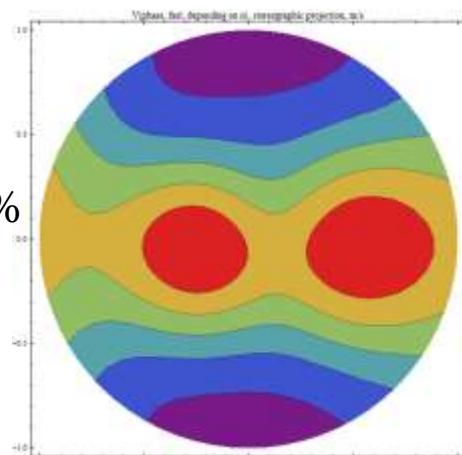
5656 m/s
6199 m/s (9.2%)
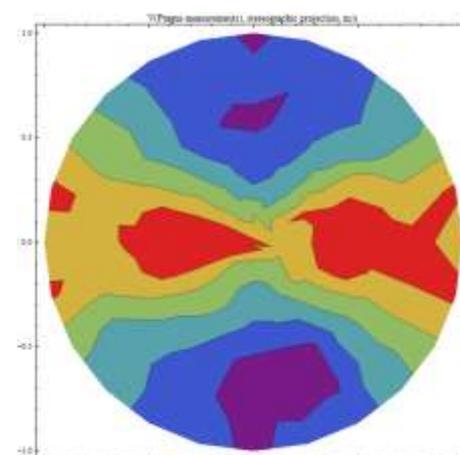
Measured
at 300 MPa

5652 m/s
6207 m/s (9.4%)

Model with 0.09 Vol%
of pores || to
muscovite grains
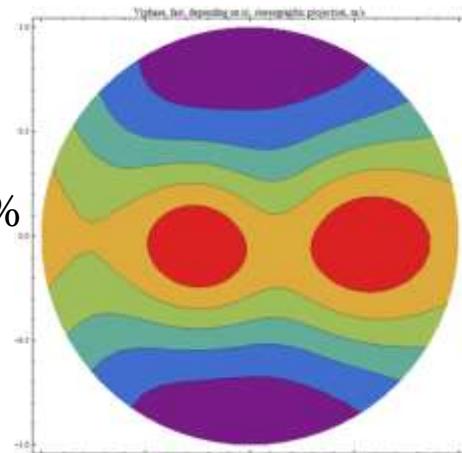
5623 m/s
6191 m/s (9.6%)
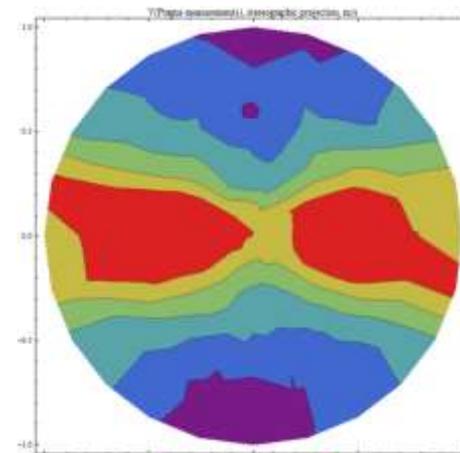
Measured
at 100 MPa

5614 m/s
6261 m/s (10.9%)

P-wave velocities,
stereographic projections,
linear scale, [m/s]

Adding pores at 0.1 MPa pressure

Model with 0.3 Vol% of pores ‖ to muscovite grains & 2 Vol% of pores ‖ to foliation
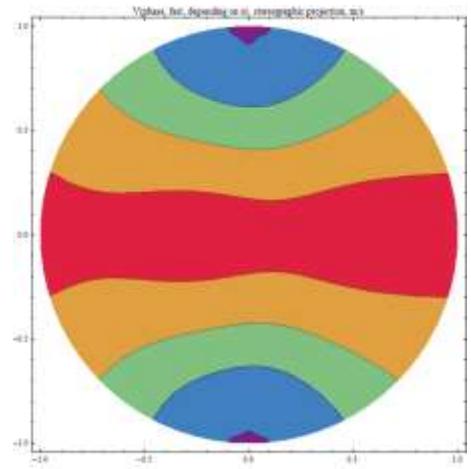
1932 m/s
5860 m/s (100.8%)

Measured at 0.1 MPa

1936 m/s
5817 m/s (100.1%)

Group velocities!

5500

4500

3500

2500
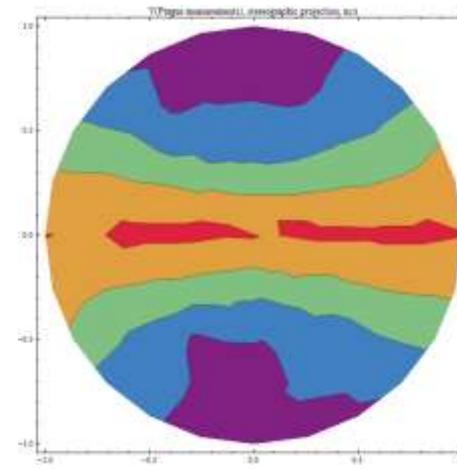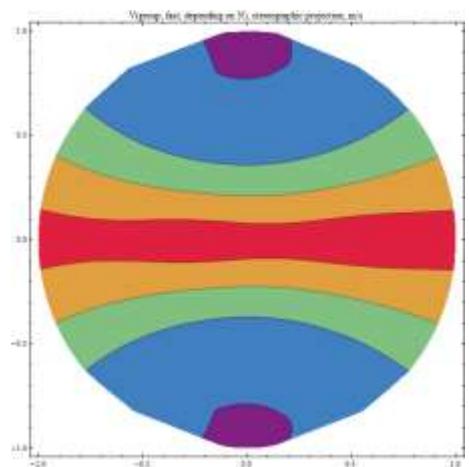
Porosity vs. pressure
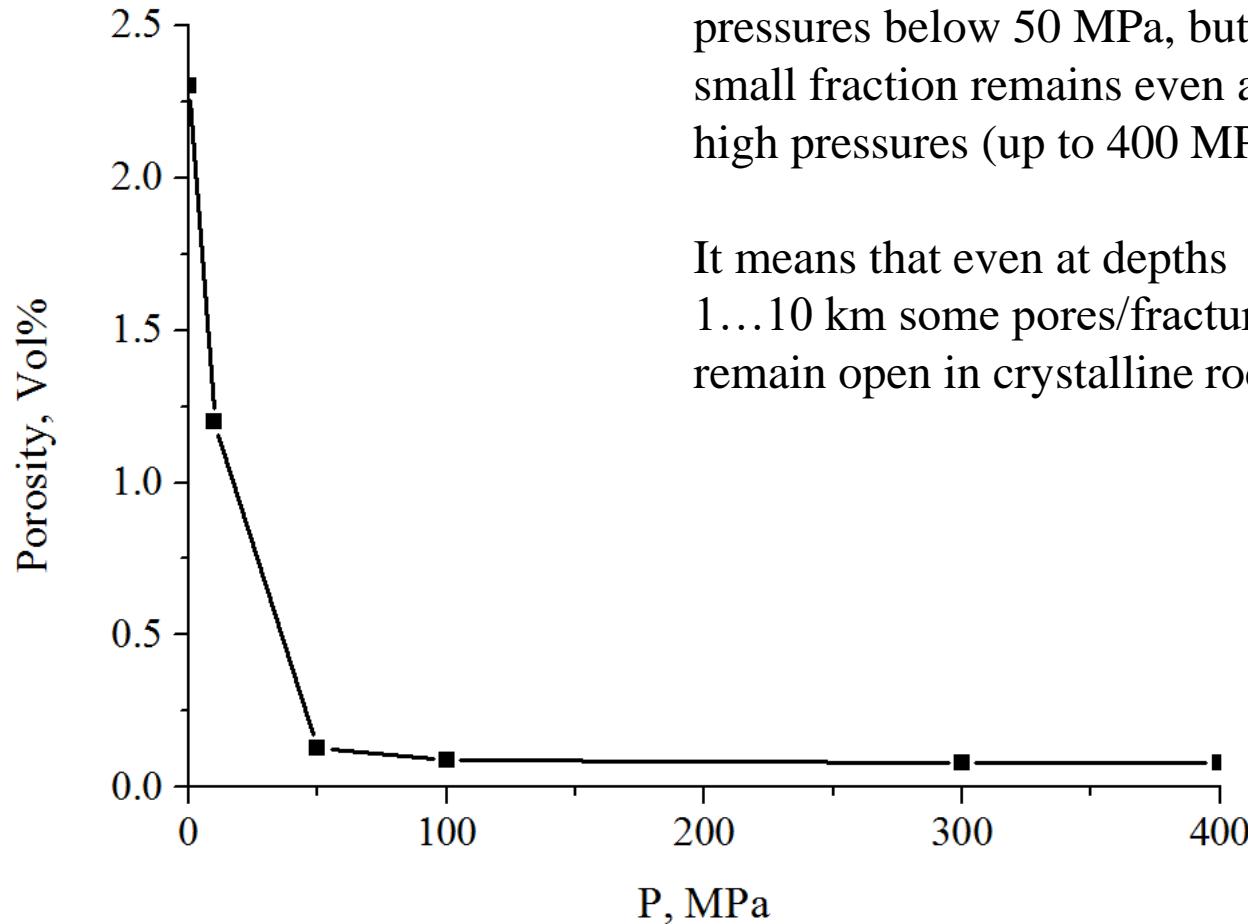
Most of pores ('meso') close at pressures below 50 MPa, but a small fraction remains even at high pressures (up to 400 MPa).

It means that even at depths 1…10 km some pores/fractures remain open in crystalline rocks.

Elastic anisotropy of rocks containing sheet silicates

- Sheet silicates are constituents of many minerals: gneisses, shales, … → interest to the seismic anisotropy.

- Distinct morphology of grains → platelets (≈ oblate spheroids). Simple common averages – Voigt, Reuss, Hill – do not really work.

- Usually it is believed that taking into account sheet silicate grain shapes will result in more elastic (seismic, if we talk about elastic waves propagation) anisotropy → not always true!

	Model biotite gneiss (no pores), based on [*Wenk et al. // Tectonophysics* **570-571** (*2012*) *123-134*, Table 3] and density of 2.75 g/cm^3		Model shale (no pores), based on [*Vasin et al. // JGR-Solid Earth* **118** (*2013*) *3931-3956*, Table 5] and density of 2.648 g/cm^3		
Grain shape of sheet silicates	Sphere {1:1:1}	Platelet {1:0.2:0.05}	Sphere {1:1:1}	Platelet {1:1:0.1}	Platelet {1:1:0.05}
V_{Pmin}, **m/s**	5551	5464	5535	5311	5285
V_{Pmax}, **m/s**	6235	6235	6366	6067	6017
k_P, **%**	11.6	13.2	14.0	13.3	12.9
ΔV_{Smax}, **m/s**	472	530	379	338	327

Elastic anisotropy of rocks containing sheet silicates
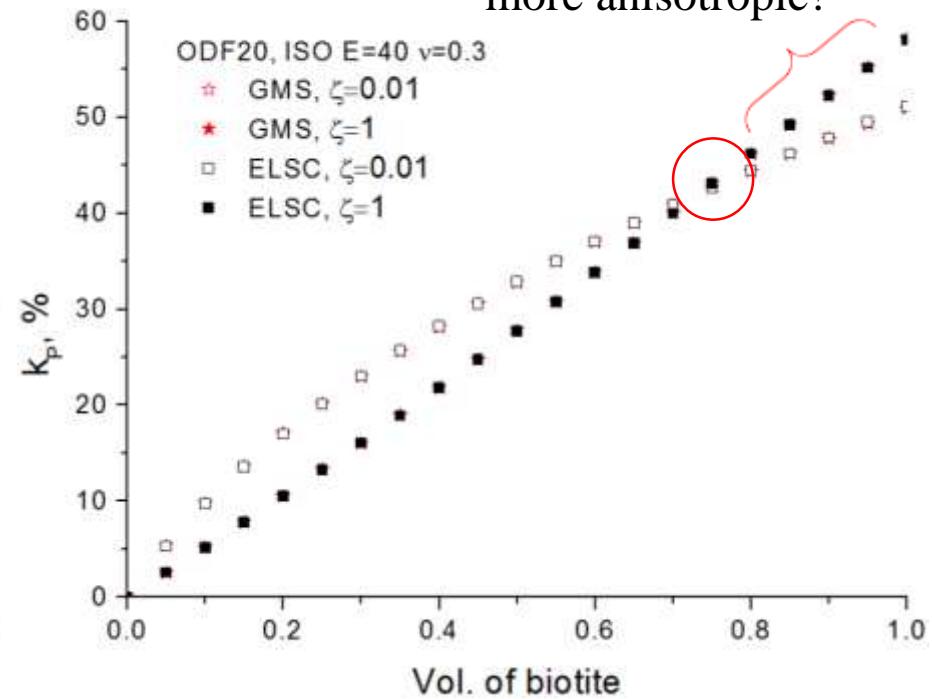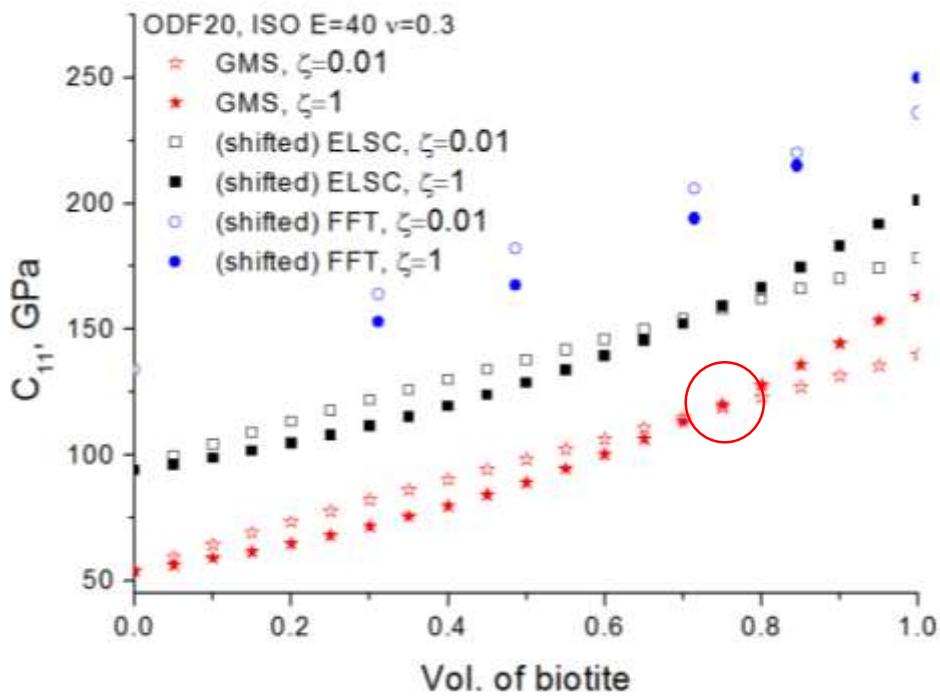
Textured biotite platelets in an isotropic matrix with Young's modulus of 40 GPa and Poisson's ratio of 0.3.

Depending on the strength of the texture and elastic properties of matrix, there is a biotite content where certain elastic constant, or wave velocities, or anisotropy coefficient do not depend on the shape of biotite inclusions.

R.N. Vasin et al. (2014) Geophysics. doi: 10.1190/GEO2014-0148.1

# Texture analysis from synchrotron diffraction experiments

If the sample is fine grained, or contains lots of hydrogen (e.g., clays), then synchrotron diffraction is the instrument of choice!

Data acquisition is really fast, even when several ω rotations are necessary.
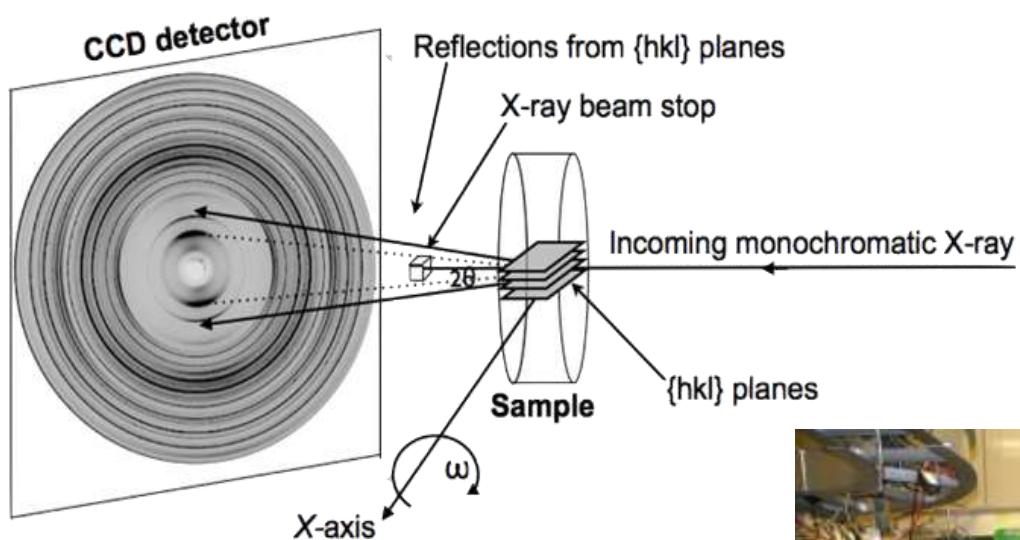
Sadly, special sample preparation is often required (cutting/polishing).
And that sample is too small for lab ultrasonic experiments.
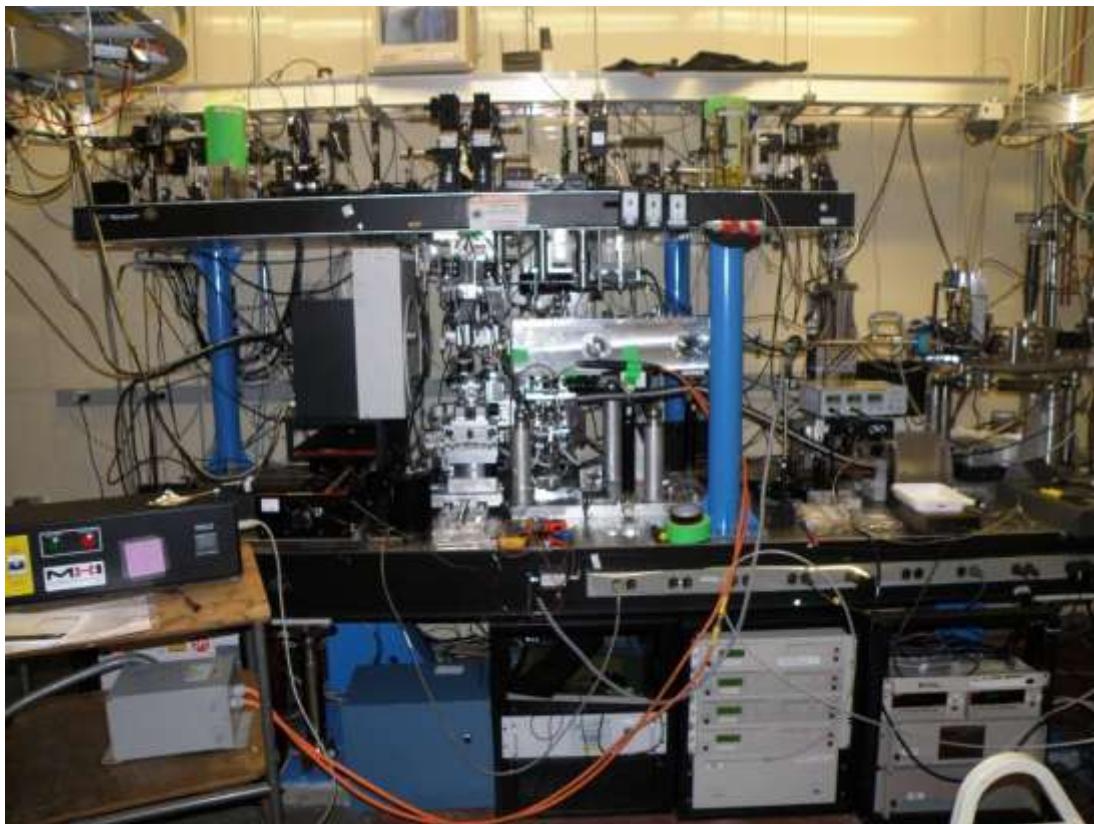
A bit of History

Origin of synchrotron radiation

It is indeed unfortunate that the informative article on synchrotron radiation in the July issue (pages 30–37) contains no reference to the original discovery of the effect, although, less relevantly and somewhat accurately, it does mention the "invention" of the betatron. Those who predicted the existence of this remarkable radiation and those who discovered it deserve recognition along with those who have since found interesting uses for it, so well described in your article.

The discovery of synchrotron radia-

with negative results. That convinced us, but not Blewett, who suggested that we look for other evidence, in particular, energy losses. We knew, in fact, that the orbit radius began to shrink when the electron energy neared 90 MeV, so that the beam would contract to target at about 106 MeV. We estimated the orbit radius at each intermediate energy by measuring the deflection current required to bring the beam to target, and found that it did indeed behave in accordance with Blewett's calculations[4] based upon the Ivanenko–Pomeranchuk hypothesis.[3] Because an alternative hypothesis (phase difference between center flux and guide field) also accounted satisfactorily for the data, no radiation had been detected, and our consultant, Marcel Schein, agreed with our objections to the Ivanenko–Pomeranchuk paper, we remained unconvinced.

Blewett correctly surmised that the radiation would be found to be distributed over a great many harmonics[4] and found support for this belief from J. Schwinger. But, with an opaque doughnut coating, complete concrete radiation shield, and closed minds, the rest of us did not see the light, literally or figuratively. We also were very busy

Synchrotron radiation from 70-MeV machine at General Electric Research Laboratory where it was first discovered in 1947.

Radiation from Electrons in a Synchrotron

F. R. ELDER, A. M. GUREWITSCH, R. V. LANGMUIR,
AND H. C. POLLOCK
*Research Laboratory, General Electric Company,
Schenectady, New York*
May 7, 1947

HIGH energy electrons which are subjected to large accelerations normal to their velocity should radiate electromagnetic energy.[1–4] The radiation from electrons in a betatron or synchrotron should be emitted in a narrow cone tangent to the electron orbit, and its spectrum should extend into the visible region. This radiation has now been observed visually in the General Electric 70-Mev synchro-

*F.R. Elder et al. (1947) Phys. Rev. **71**, 827-828.*
G.C. Baldwin & D.W. Kerst (1975) Physics Today, doi: 10.1063/1.3068762

A bit of History

Synchrotron Radiation as a Source for X-ray Diffraction

G. ROSENBAUM & K. C. HOLMES
Max-Planck-Institut für Medizinische Forschung, Heidelberg

J. WITZ
Laboratoire des Virus des Plantes, Institut de Botanique de la Faculté des Sciences de Strasbourg, Strasbourg

DESY, Hamburg

Diffraction from flight muscle fibers of water bug *Lethocerus maximus*
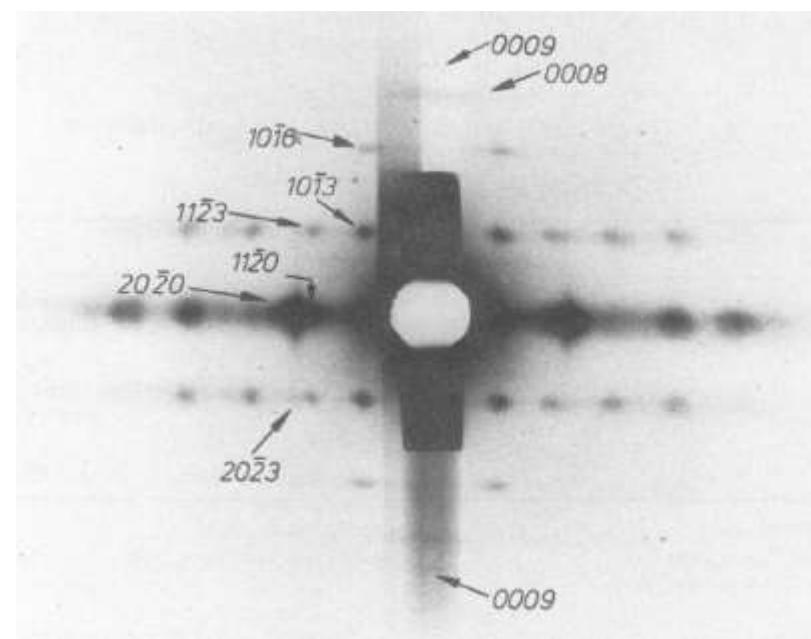
*G. Rosenbaum et al. (1971) Nature **230**, 434-437.*   *R.S. Goody et al. (1975) Biophysical J. **15**, 687-705.*

Киммериджский сланец

Сланцы – осадочные горные породы, часто являются кровлей или вмещающими породами для нефтяных/газовых месторождений. Свойства интересны: георазведка, добыча/оценка запасов, захоронение отходов.

Киммериджский сланец, сформировавшийся в Юрском периоде (≈ 155 млн. лет); получен из скважины в Северном море с глубины 3750 м под уровнем моря.

Один из немногих, для которых упругие свойства изучены и доступны (сланец поперечно изотропен → пять упругих констант). *B.E. Hornby (1998) J. Geophys. Res. **103**, 29945-29964.*


(d)   100 μm
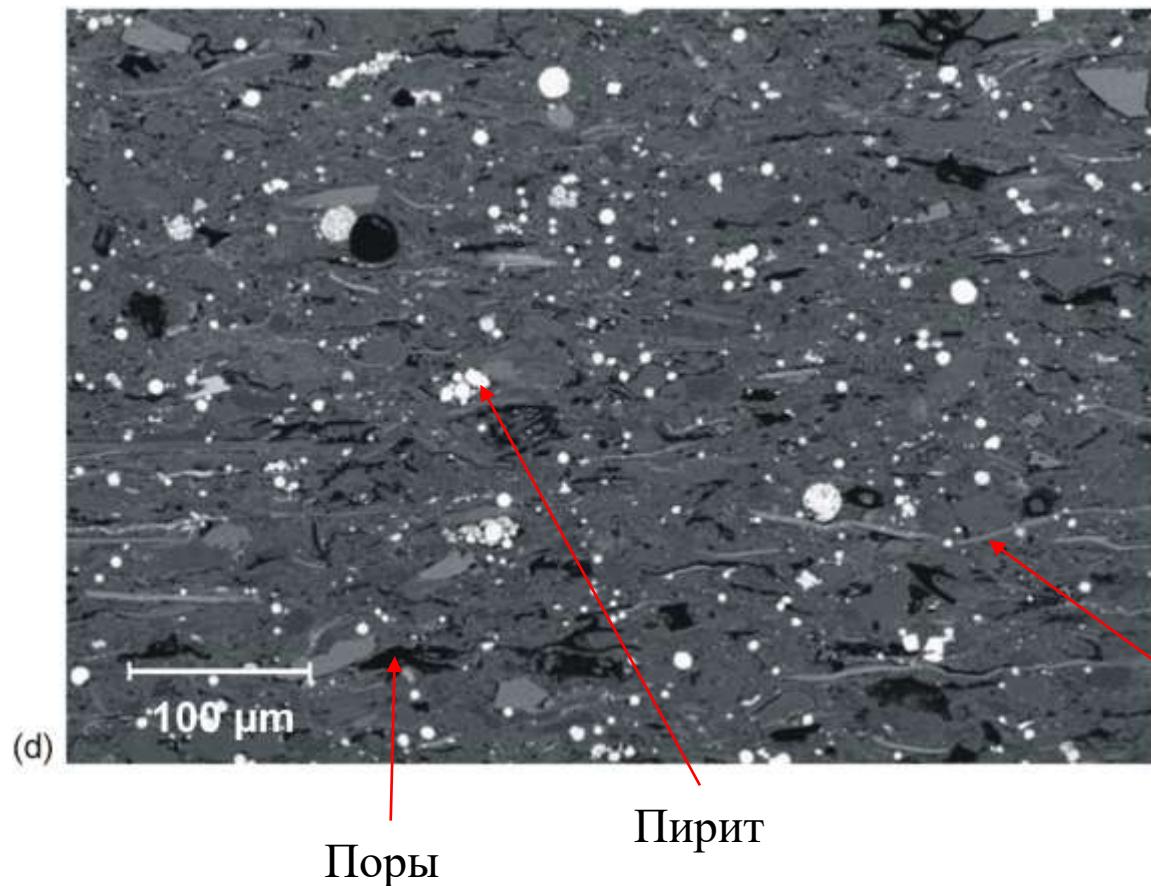
*R.N. Vasin et al. (2013) J. Geophys. Res. doi:10.1002/jgrb.50259*

Поры

Пирит

Слюда (illite-mica)

Форма зёрен и пор
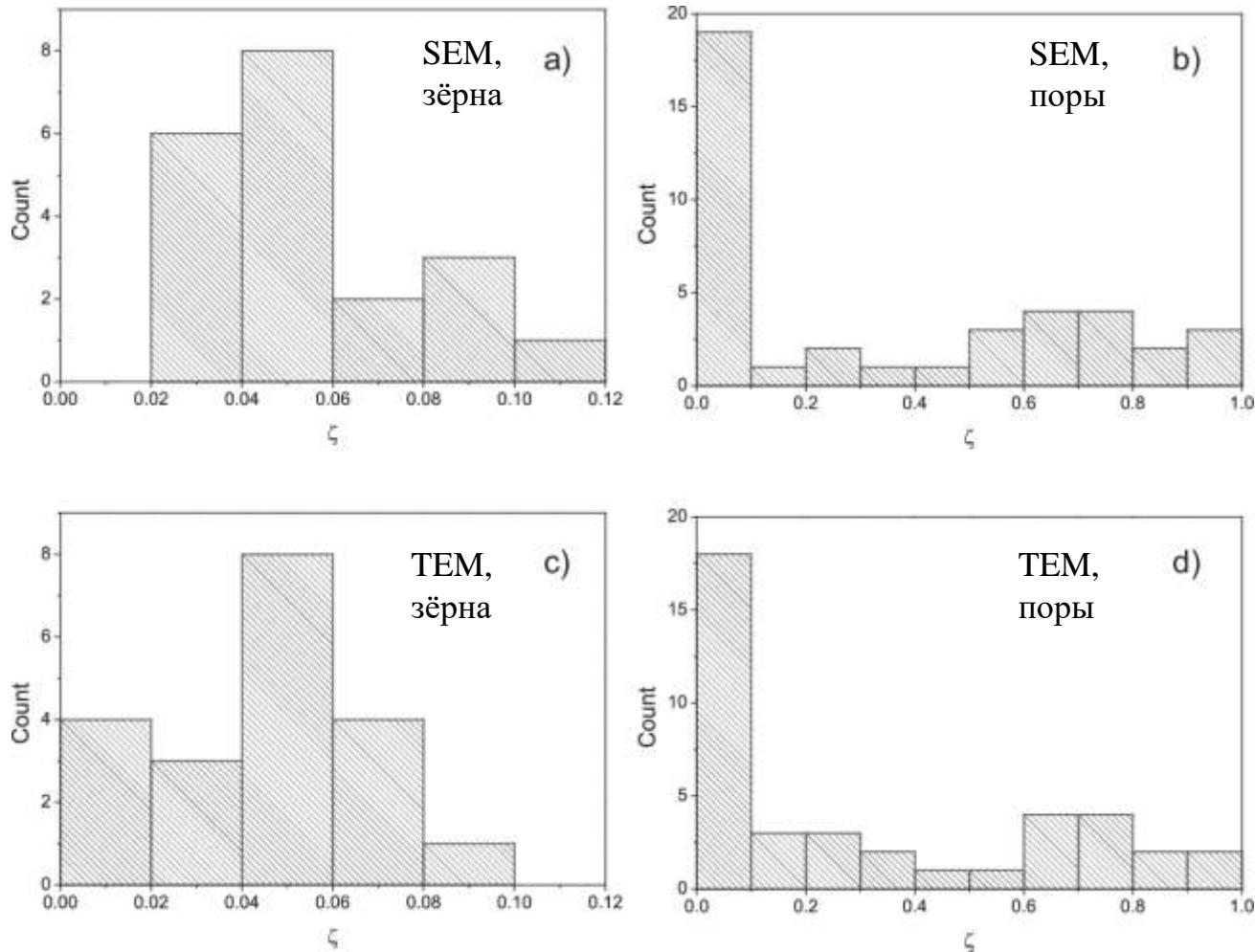
Распределения зёрен слоистых силикатов и пор по форме.

К сожалению, учитывать эти распределения слишком сложно; можно пользоваться некими средними параметрами: {1:1:0.05} для зёрен, {1:1:0.01} + {1:1:1} для пор.

Плоские поры ≈ параллельны плоским зёрнам слоистых силикатов.

Дифракционный эксперимент
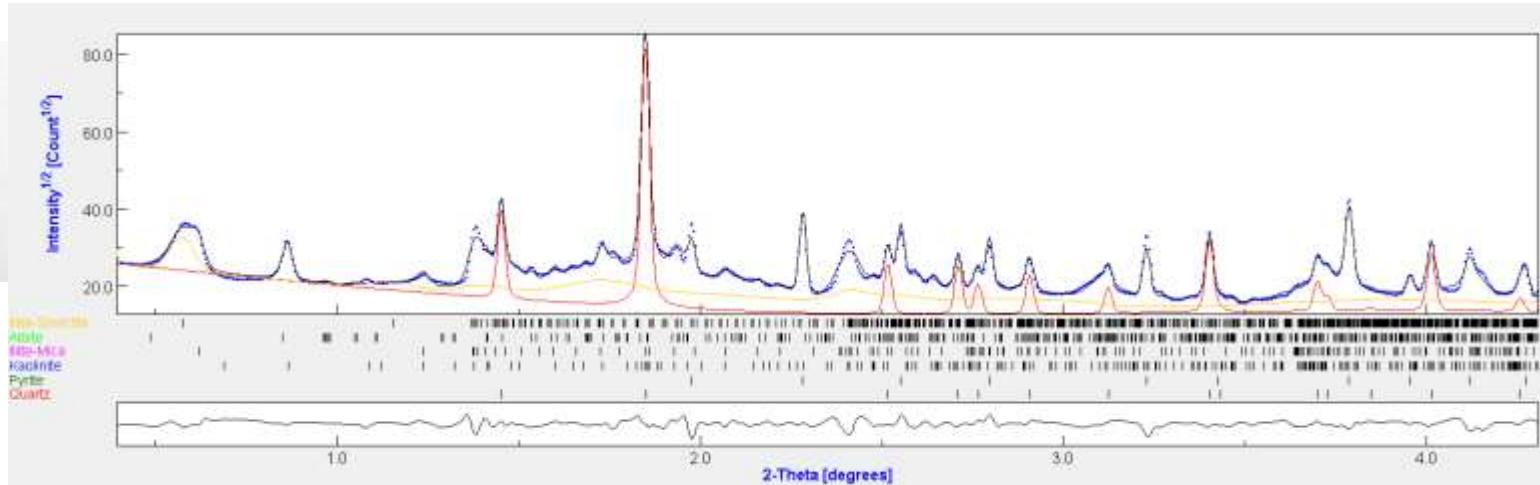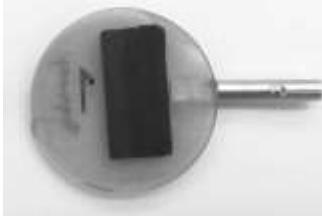
Иллит-смектит: турбостратный беспорядок
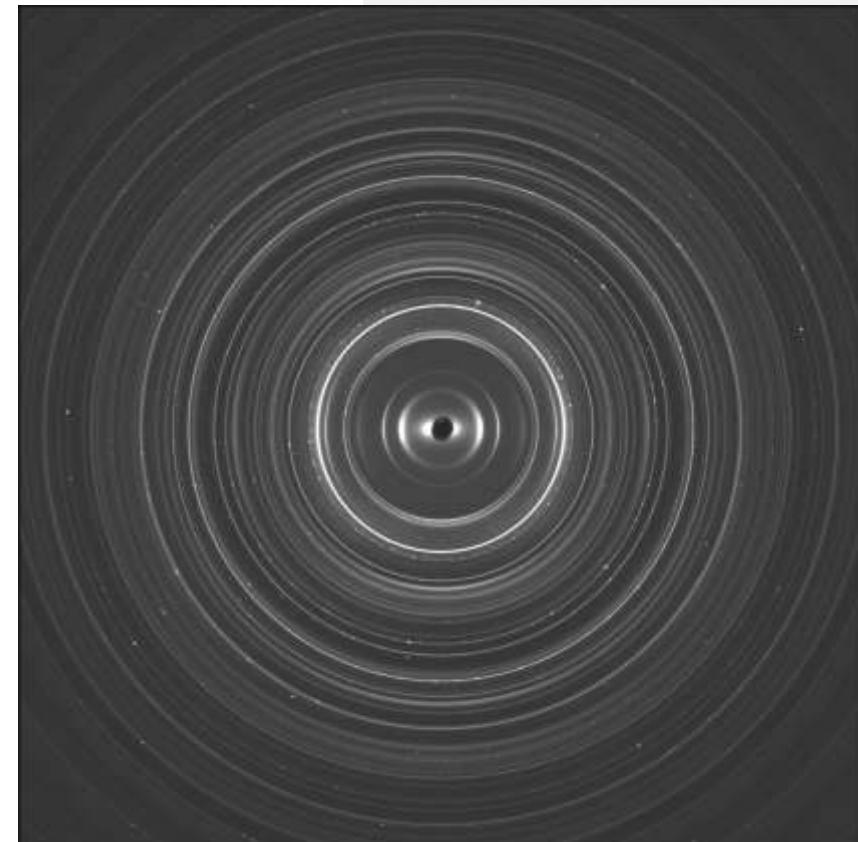
Mineral	Vol%	Wt%
Quartz	25.1	23.6
Albite	3.7	3.4
K-feldspar	-	-
Pyrite	4.4	7.8
Kaolinite	8.9	8.0
Illite-smectite	29.9	29.3
Illite-mica	28.0	27.9
Chlorite	-	-

Дифракционный эксперимент: распределение зёрен минералов по ориентациям
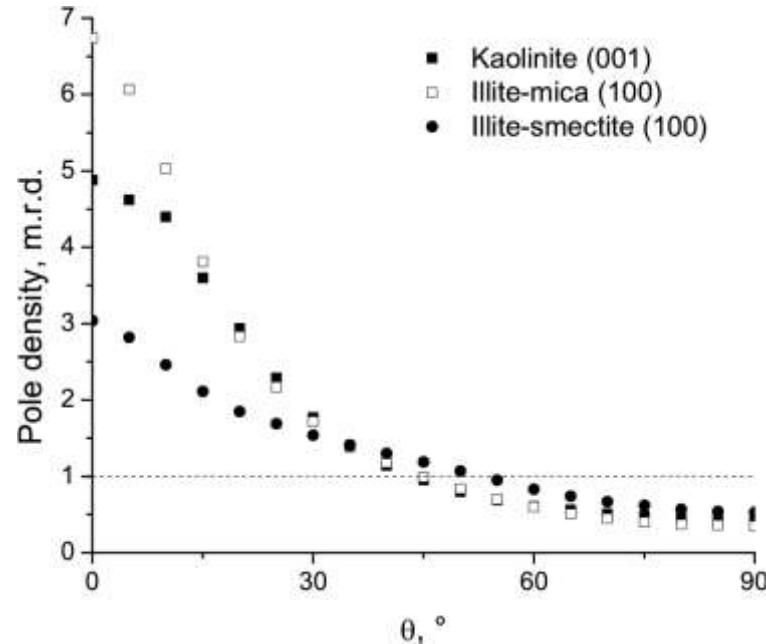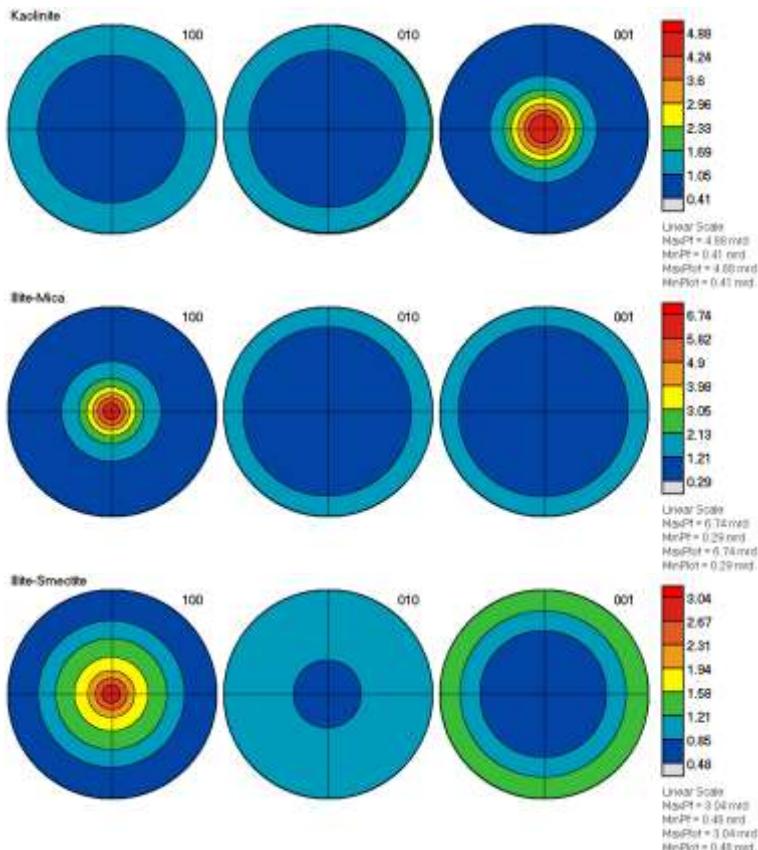
Mineral	f_{min}	f_{max}	F_2	FWHM, °
Kaolinite	0.19	5.67	1.86	45
Illite-mica	0.25	6.74	2.09	36
Illite-smectite	0.42	3.04	1.26	57

Равноплощадные проекции на плоскость фолиации.

Текстуры аксиально симметричны, поскольку сформированы осаждением (sedimentation).

Большие f_{min}! (Обычно считаются =0…)

Кварц, альбит, пирит – хаотическое распределение зёрен.

Пористость?

- [*Hornby, 1998*] – 2.5 об.% пор (замещение гелием) при атмосферном давлении, около 1.5 об.% при 80 МПа (оценка).
- Плотность при 80 МПа равна 2.648 г/см³ (не приводится в статье, получена из сопоставления скоростей упругих волн с упругими модулями); объёмные доли + плотности минералов дают плотность 2.854 г/см³, т.е. 7.2 об.% 'пустых' или 11.1 об.% водонасыщенных пор.
- Синхротронная томография: 6.3 об.% включений с низкой плотностью (пустоты, флюиды, органические включения). Не учитывает поры размером менее 1 мкм, которые видны на картинках ТЕМ. Однако при повышенных давлениях по крайней мере часть пор закрыта (особенно 'пустые').

(a) 50 μm
(b) 50 μm
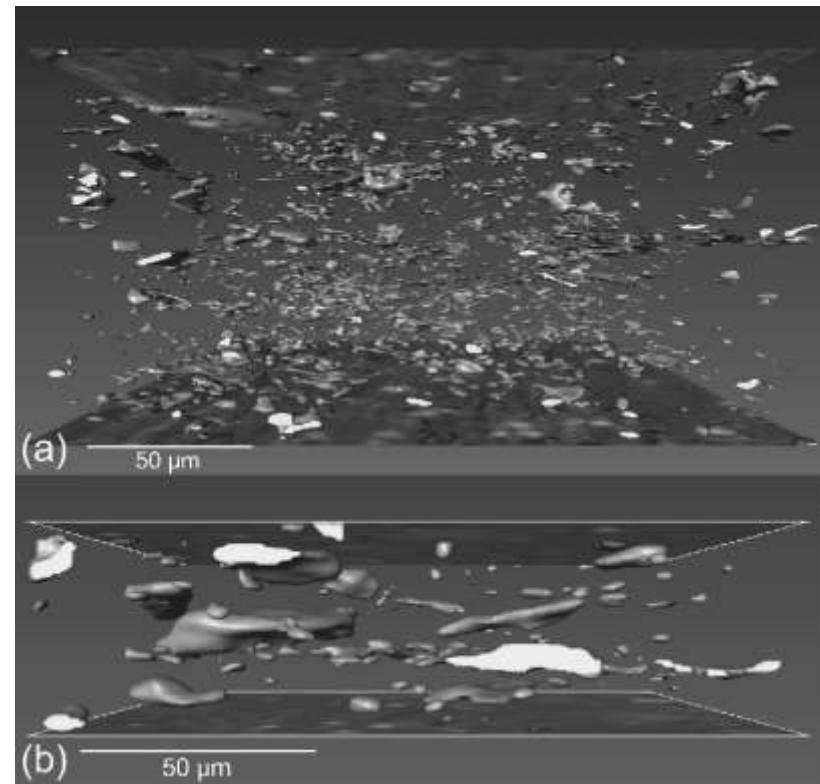
Для 'пустых' пор плотность =0, упругие модули =0.
Для водонасыщенных пор плотность равна 1 г/см³, модуль объёмного сжатия = 2.2 ГПа (≈ такой же у нефти и органических включений).

Скорости упругих волн в сланце: эксперимент
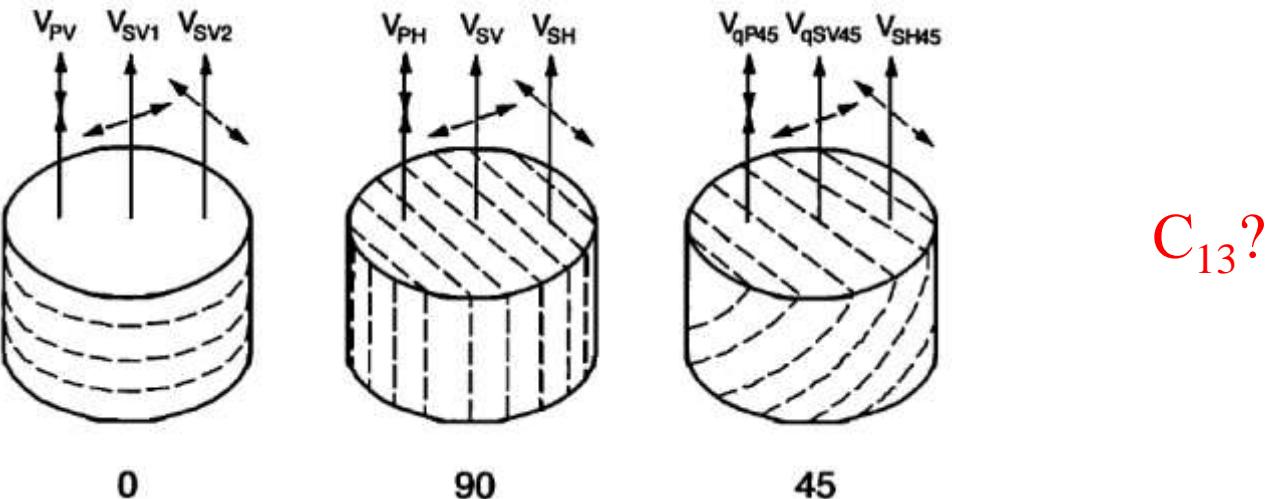
C_{13}?

$$V_{PV} = \sqrt{\frac{C_{33}}{\rho}} \qquad V_{SH} = \sqrt{\frac{C_{66}}{\rho}} \qquad V_{SV1} = V_{SV2} = V_{SV} = \sqrt{\frac{C_{44}}{\rho}} \qquad V_{PH} = \sqrt{\frac{C_{11}}{\rho}} \qquad V_{SH30} = \sqrt{\frac{3C_{44} + C_{66}}{4\rho}}$$

$$V_{qP30} = \sqrt{\frac{C_{11} + 3C_{33} + 4C_{44} + \sqrt{C_{11}^2 + 12C_{13}^2 + 9C_{33}^2 + 16C_{44}^2 + 4C_{11}C_{44} + 24C_{13}C_{44} - 6C_{11}C_{33} - 12C_{33}C_{44}}}{8\rho}}$$

$$V_{qSV30} = \sqrt{\frac{C_{11} + 3C_{33} + 4C_{44} - \sqrt{C_{11}^2 + 12C_{13}^2 + 9C_{33}^2 + 16C_{44}^2 + 4C_{11}C_{44} + 24C_{13}C_{44} - 6C_{11}C_{33} - 12C_{33}C_{44}}}{8\rho}}$$

B.E. Hornby (1998) J. Geophys. Res. **103**, *29945-29964.*

Упругие константы сланца: модели

#	C_{11}	C_{13}	C_{33}	C_{44}	C_{66}	Remarks
A	56.2	20.5	36.4	10.3	18.9	$^{exp}C_{ij}$ at 80 MPa [*Hornby, 1998*]
C	56.0	16.3	36.3	10.6	19.2	GMS, 6.5 Vol.% pores

#	C_{11}	C_{13}	C_{33}	C_{44}	C_{66}	Remarks
G	48.4	16.4	27.3	7.8	17.0	$^{exp}C_{ij}$ at 5 MPa [*Hornby, 1998*]
J	46.3	12.9	27.6	8.3	16.0	GMS, 7.3 Vol.% pores

Плоские поры приблизительно параллельны зёрнам слоистых силикатов.
Из анализа ФРО слоистых силикатов и их объёмных долей получается, что 31.2 об.% слоистых силикатов хаотически ориентированы. Т.е. модельная ФРО для плоских пор должна иметь фон ≈ 30% + должна быть аксиально симметричная ≈ гауссова компонента с шириной около средней ширины ФРО слоистых силикатов ИЛИ несколько острее, т.к. есть макроскопическая плоскость фолиации и связанные с ней трещины/мезо-поры.

Модель с 3.5 об.% плоских пор и 3 об.% сферических описывает C_{IJ} сланца при 80 МПа.
Модель с 4.3 об.% плоских пор и 3 об.% сферических описывает C_{IJ} сланца при 5 МПа.

В итоге, изменение упругих свойств сланца с глубиной, в принципе, описывается 1 параметром – количеством плоских пор.

Спасибо за внимание!